11-23-2020 11:00 AM

Simulation of Operational Extreme Wind Conditions for Horizontal Axis Wind Turbines Based on IEC Standard

Kamran Shirzadeh Ajirlo, *The University of Western Ontario*

Supervisor: Hangan, Horia M., *The University of Western Ontario*
Co-Supervisor: Crawford, Curran, *University of Victoria*
A thesis submitted in partial fulfillment of the requirements for the Master of Science degree in Mechanical and Materials Engineering

Recommended Citation

Shirzadeh, Kamran Ajirlo, "Simulation of Operational Extreme Wind Conditions for Horizontal Axis Wind Turbines Based on IEC Standard" (2020). *Electronic Thesis and Dissertation Repository*. 7495.
https://ir.lib.uwo.ca/etd/7495

Abstract

The possibility of simulating deterministic extreme operational conditions for horizontal axis wind turbines based on the IEC 61400-1 standard in the WindEEE Dome at Western University was investigated. WindEEE has 60 fans (a matrix of 4 by 15 with 0.8m diameter each) on one of the walls to generate straight and sheared flows. These fans were controlled by their power set-points and by their adjustable Inlet Guiding Vanes (IGV) to generate the Extreme Operational Gust (EOG), positive and negative Extreme Vertical Shear (EVS), and Extreme Horizontal Shear (EHS) cases as per IEC 61400-1 standard to be further applied for testing a scaled 2.2 m Horizontal Axis Wind Turbine (HAWT). First, Computational Fluid Dynamics (CFD) simulations of the WindEEE test chamber were carried out in order to predict the fans setups for each of these extreme conditions. The experiments were then carried out using these settings and a comparison was performed between the resulting flow field time histories and the prescribed conditions from the standard. The results showed a successful simulation of these extreme conditions. The extreme conditions were then applied to investigate the power and load performance of the scaled HAWT. The results revealed that the unsteady shears had no significant impact on the overall power generation. EHS induced a significant twisting moment on the structure. The EOG has the most noticeable effect which highly depends on the operational tip speed ratio (TSR) of the wind turbine and the time duration of the event.

Keywords

Extreme operational Gust, Extreme Shear, HAWT, IEC Standard, Wind Tunnel Experiment.

Summary for Lay Audience

The main goal of this study is to develop a physical simulation of simplified extreme wind conditions (extreme operational gust and extreme wind shears) that are dynamic and defined by a standard for wind turbines; then investigate the effect of these extreme conditions on overall performance of a model wind turbine. Being able to simulate these dynamic flow fields can be a contribution for future scholars working in the wind energy area to make these wind energy systems more reliable and predictable by bringing the possibility of experimental validation for computer simulations of these transient events and their effects on wind turbines. All these together can help accelerate the decreasing price of energy being produced by these machines.

Co-Authorship Statement

Chapter two is a journal article submitted to journal of Wind Energy Sciences, under co-authorship of K. Shirzadeh, H. Hangan and C. Crawford. In this chapter the numerical studies were developed by the lead author (K. Shirzadeh) under direct supervision of C. Crawford at IESVic (Institute for Integrated Energy Systems University of Victoria) then the experiments were designed and conducted by the lead author with supervision of H. Hangan. For this chapter, all authors thank Gerald Dafoe and Tristan Cormier for helping with the measurement setups. This part of work is supported by the UWO, NSERC.

Chapter three is a journal article submitted to journal of Wind Energy Sciences, under co-authorship of K. Shirzadeh, H. Hangan, C. Crawford and P. Hashemi Tari. The lead author designed and conducted the experiments under supervision of H. Hangan and then completed the data analysis with comments from all the co-authors. For this chapter, all authors thank Gerald Dafoe and Tristan Cormier for helping with the measurement setups. This chapter is supported by the WindEEE Dome CFI Grant and by NSERC Discovery Grant R2811A03.

Acknowledgments

I would like to express my sincere gratitude to my supervisor, Dr. Horia Hangan for his valuable advices and insights throughout the research.

I wish to express my appreciation for my co-supervisor Dr. Curran Crawford for his continuous encouragement and supports. Special thanks to the IESVic staff and students that welcomed me during my four-month visiting period from beautiful Victoria University.

I would like to show my gratitude to the WindEEE staff, Adrian Costache, Gerry Dafoe, Tristan Cormier, Priscilla De Luca, Elisa Yaquian who helped me to bring my imaginations and thoughts to the real world.

I like to thank my bachelor supervisors Dr. Pooyan Hashemi Tari and Dr. Kobra Gharali firstly to believing in me, secondly their constant supports to help me grow in all aspects of my life and thirdly for recommending me to my current supervisor Dr. Horia Hangan.

I gratefully thank my friends and colleagues Dr. Chowdhury Jubayer, Dr. Djordje Romanic, Dr. Mohammad Karami, Dr. Malihe Mehdizadeh, Arash Ashrafi, Aya Kassab, Anant Gairola, Daniel Davalos, Juan Pablo Lopez, Gabriel Narancio, Zahra Habibi, Marelina Enus, Federico Canepa, Andrea Ballestracci, Hiroaki Shoji, Shiyu Zhao, Chowdhurry Junayed, and Hossain Tanjil for all the help and friendship I received throughout these past two years with lots of ups and downs.

Lastly, I like to thank my parents, Mohammad and Ashraf, and my brothers, Kaveh and Siamak, who did all they could to support me throughout this experience.

Table of Contents

List of Tables

List of Figures

Nomenclature

C_p	Power Coefficient (-)
F_D	Drag force on blade element
F_L	Lift force on blade element
M_x	Moment around x-axis (Nm)
M_y	Moment around y-axis (Nm)
M_z	Moment around z-axis (Nm)
U_∞	Upstream free velocity $(\frac{m}{s})$
U_{e1}	Extreme wind speed with 1 year return period $(\frac{m}{s})$
U_{e50}	Extreme wind speed with 50 years return period $(\frac{m}{s})$
U_{gust}	The gust magnitude $(\frac{m}{s})$
U_{ref}	A reference velocity $(\frac{m}{s})$
Z_0	Roughness height (m)
z_{ref}	A reference height (m)
D	Diameter of the rotor (m)
t	Instantaneous time (s)
T	Gust time duration (s)

U	Wind speed $(\frac{m}{s})$
A	$Area\ of\ the\ rotor\ (m^2)$
L'	The length of one loop of the tip vortex helix (m)
P	Power (W)
R	Radius of the rotor (m)
T'	The propagation time of one tip vortex helix (s)
Z	Height (m)
$\boldsymbol{L}$	Length of the four loops of the tip vortex helix (m)

Greek Symbols

Λ_u	Streamwise turbulence length scale (m)
σ_u	Standard deviation of the turbulent wind in streamwise direction (m/s)
Φ	Angle of incident with the rotor plane at specific radius (rad)
α	Angle of attack relative to airfoil (rad)
β	Pitch angle at the specific blade element/ radius (rad)
λ	Tip Speed ratio (-)
ρ	Air density $(\frac{kg}{m^3})$
ω	Angular velocity of the rotor $(\frac{rad}{s})$

Chapter 1

1 General introduction

1.1 Climate change

The Earth's climate has been changed throughout the history. Just in the last 650,000 years there have been seven cycles of glacial advance and retreat. Most of these climate changes are related to very small variations in earth’s orbit that change the amount of solar energy our planet receives. The current warming trend that most likely is the result of human activities since the industrial revolution (mid-18th), proceeds at a rate that never existed before. The main problem with human activities is the production of the greenhouse gases (GHG) like carbon dioxide and methane which are able to trap the heat inside their molecules (see Figure 1-1). With the current increasing trend of the human population and demand, the capability of the natural ecosystems are being challenged [1]. The technological advances have enabled scientists to collect various types of information from our planet in global scale. These data show the planet’s average surface temperature has risen 0.9 ℃ since late 19th; the top layer of oceans warmed 0.2 ℃ and the ocean acidity increased 30% since mid-20th [2]. The global sea level rose 8 inches in the last century with an increasing pace which is due to melting of the ice sheets, glaciers and the snow covers, especially in northern hemisphere. The number of extreme weather conditions such as high temperature events and intense rain falls have increased in the recent decades [3].

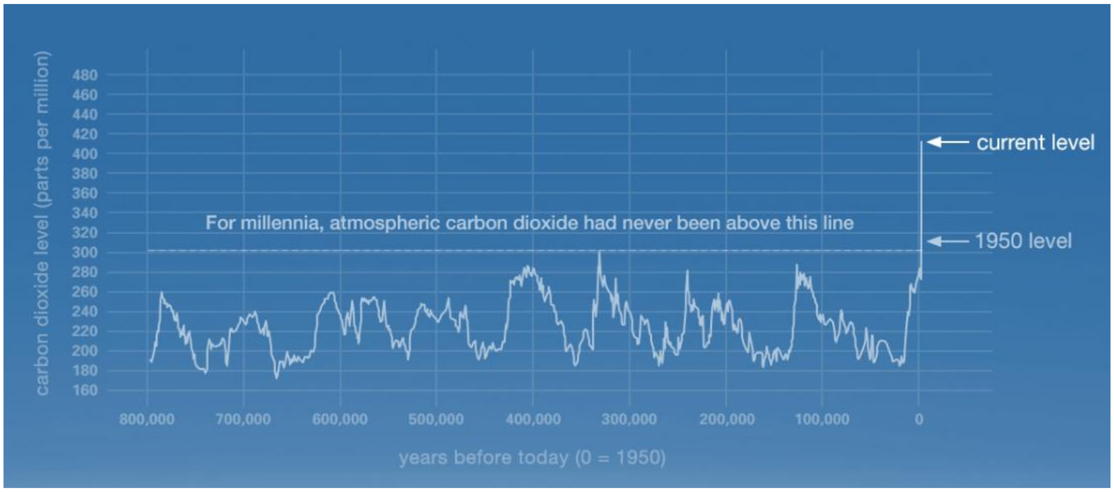

Figure 1-1: The carbon dioxide level in atmosphere based on the comparison of atmospheric samples contained in ice cores provides evidence that atmospheric CO2 has increased since the industrial revolution [4]. The graph has been adopted from [5].

The second major GHG, methane, is more efficient at trapping heat than a molecule of carbon dioxide but it has shorter life cycle. Pinpointing the source of methane is more difficult. Methane can be generated from fossil fuel, agricultural, biomass burning, biofuels and wetland sources [6]. Recent studies show that hydroelectric dams can be a considerable source of methane. Continuously falling and rising water levels at the reservoir behind the dam results in anaerobic digestion of the vegetations which produce methane [7].

The transition to renewable energy sources from fossil fuels is not a choice nevertheless, it is the only way for humankind to have a sustainable future on this planet. This should happen for two main reasons, first is that the sources of fossil fuels are limited. The second is to maintain a healthy environment. On top of that, renewable energies are beneficial in terms of energy security and distributed power generation which are essential from a geopolitical and energy efficiency point of views [8]. Especially with current technological advancements that made these sources of energy cost effective and feasible

1.2 Canada electricity outlook

Canada generated an estimated 651 billion kilowatt-hours (kWh) of electricity in 2017, with large share of hydro power and nuclear power and just 7% from renewable sources (see Figure 1-2), despite having a great potential in this section [9].

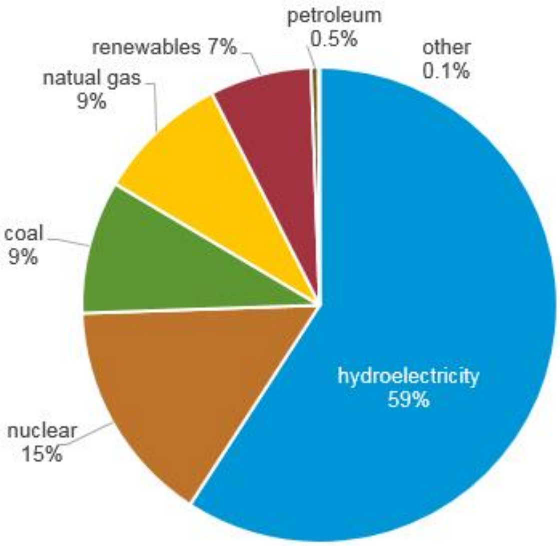

Figure 1-2: Share of Canada electricity generation by fuel in 2017 [9]

Figure 1-3 shows the Canada's annual mean wind energy density at 80m above the ground. Accordingly, four main high potential wind power regions in the order are the east and west coasts; the Hudson Bay area and its surroundings; the southern parts of the Ontario, Manitoba, Saskatchewan and Alberta [10].

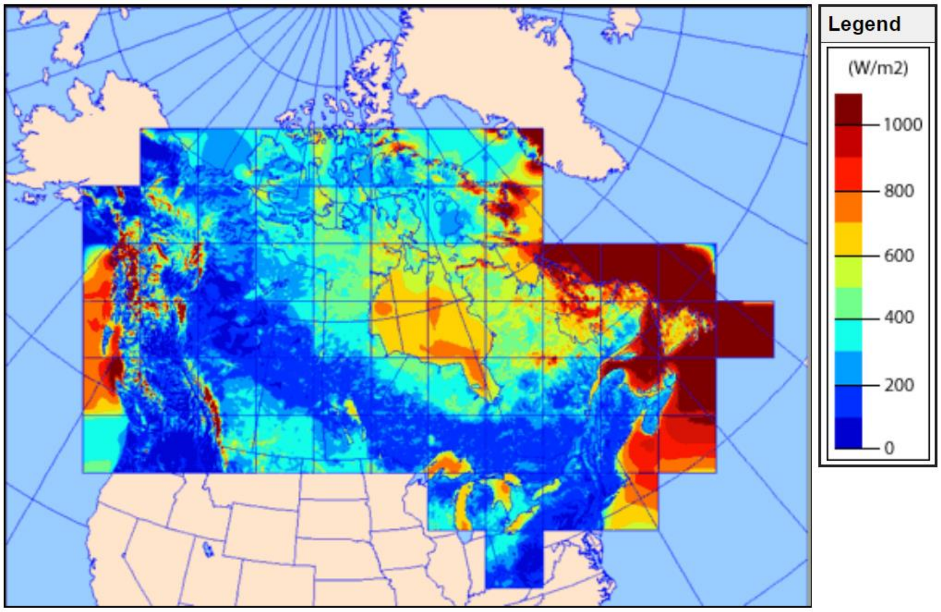

Figure 1-3: Canada's annual mean wind energy density map at 80m height [10]

With the continuing growth of installed capacity of the wind energy systems, Canada ended up having 13,413 MW of onshore wind capacity (Figure 1-4a) at the end of 2019, where Ontario has the highest share (about 5.5 GW see Figure 1-4b) [11].

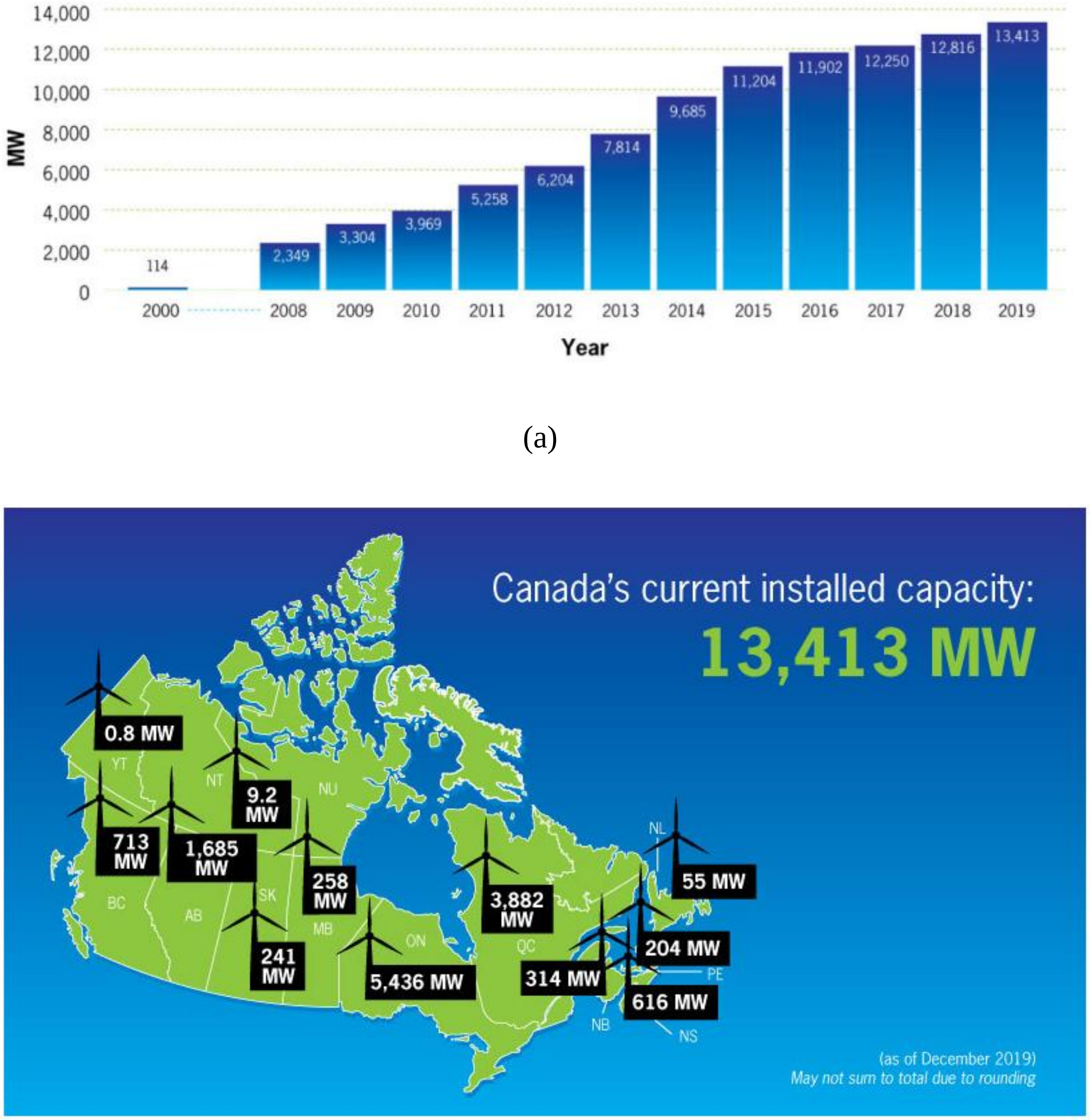

(a)

(b)

Figure 1-4: The installed wind energy capacity, (a) the total growth trend from beginning of the century, (b) the installed capacity at each province by end of 2019 [11]

As mentioned earlier, in Canada, hydropower has the most installed capacity for electricity generation due to accessibility to large amount of water resources. Figure 1-5 shows the trend of installed capacity of clean energy sources in Canada from 2010. Accordingly, the share of hydropower remained relatively the same throughout the past decade ($\sim 75\ GW$).This is due to saturation in the hydropower market as well as price reduction of other sources of energy. Based on the growth trend of the wind in the recent decade, in comparison with the other sources, wind energy may have the highest share of the energy sector market in near future.

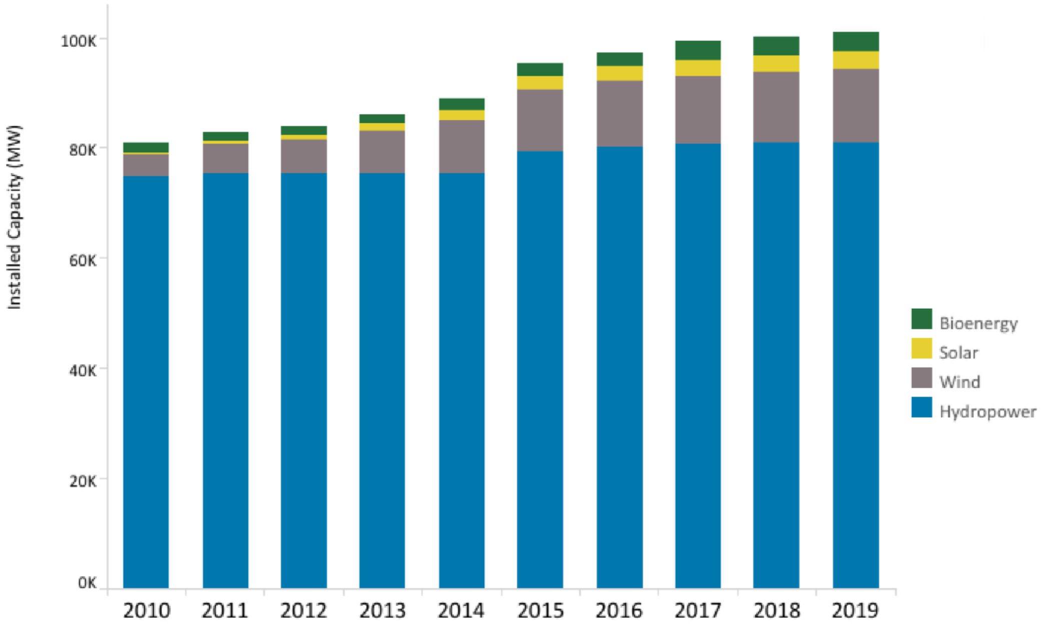

Figure 1-5: The trend of total installed capacity of new energy sources [9]

In order to have fair comparison for the energy price per kWh from different sources the LCOE (Levelized Cost of Electricity) is being used. It represents the present value of the total cost of building and operating a power generating plant over an assumed financial life and duty cycle, converted to equal annual payments and expressed in terms of real dollars to remove the impact of inflation [12]. Figure 1-6 shows the globally averaged cost of energy in 2010 comparing with 2018 for different energy sources with the effect of project size. By comparing Figure 1-5 and Figure 1-6, the correlation between the installed power and the cost of energy is intuitive. Throughout the decade, the cost of wind and solar energies are dropping fast. The price of hydropower remained relatively the same while it still remains the cheapest option. Therefore, more likely the next largest market in the energy sector in Canada would be the wind energy due to vastly accessible high potential lands and shores.

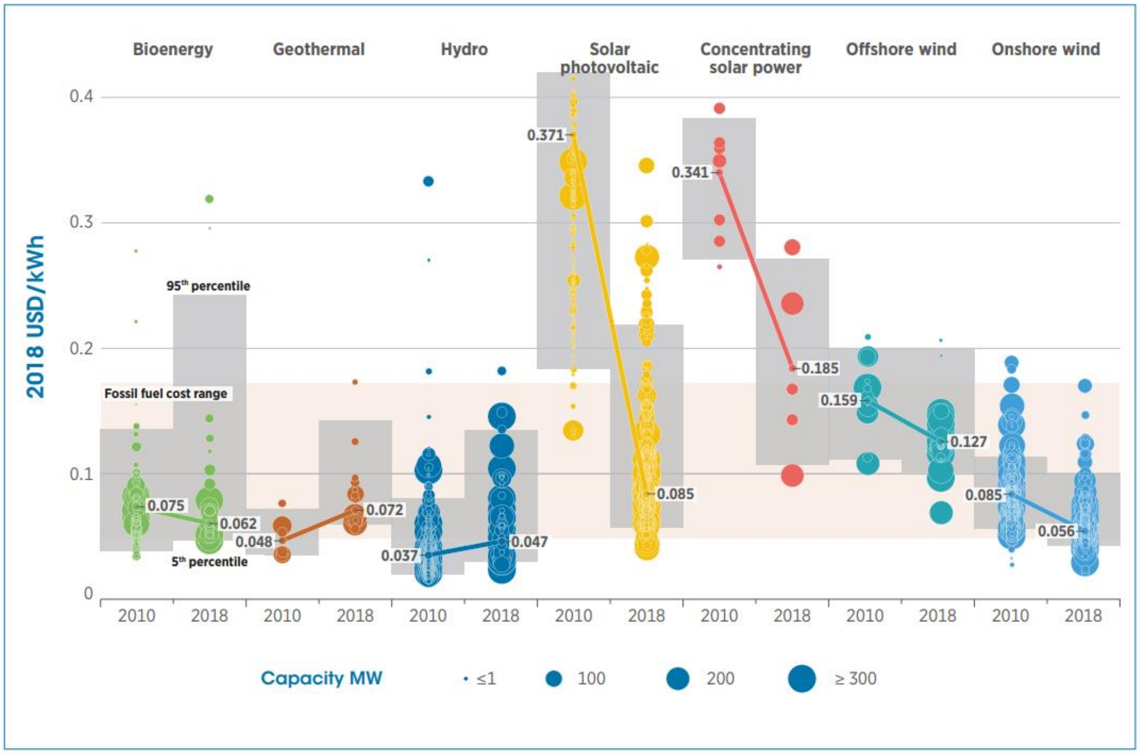

Figure 1-6: The comparison of globally averaged LCOE between 2010 and 2018 for various type of energy including the effect of the project size, the wind and solar energy price trends look highly promising [13]

1.3 Horizontal axis wind turbines

Horizontal Axis Wind Turbines (HAWT), as the name applies, are wind energy systems for which the axis of rotation of the rotor is horizontal and parallel to the main wind direction. Out of all wind energy devices, HAWTs have proved to be the most cost efficient and therefore they dominate the total installed capacity. The main components of this type of turbines are the blades which are connected to the main shaft at hub; a nacelle that contains the gearbox, generator and other electronical equipment; a steel tubular tower and the foundation. The general layout of an upwind HAWT is presented in Figure 1-7.

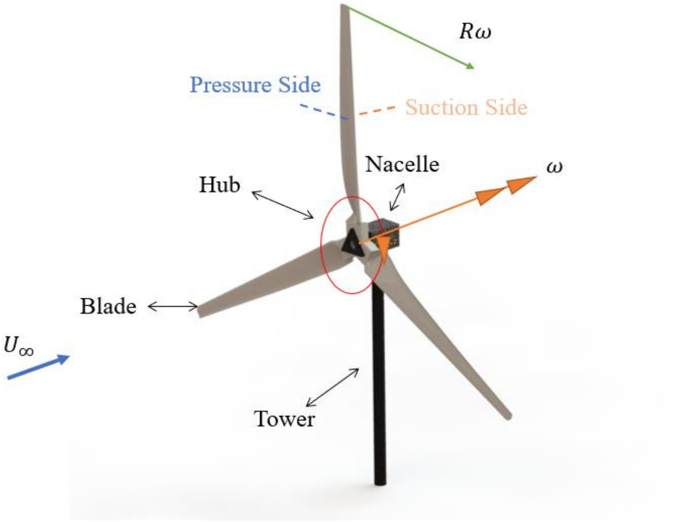

Figure 1-7: upwind HAWT layout

The blades have the specially chosen airfoil shapes with different chord sizes and pitch angles throughout their span [14]. As the wind passes through the rotor a pressure difference happens at the pressure side and suction side of the blade (Figure 1-7). The integral of these pressure differences creates a net torque on the rotor and thus to the main shaft and as the result, the rotor starts spinning and generating work and power. Essentially the blades generate torque from the tangential component of the lift force (F_L) while the normal component creates an axial force (thrust) on the rotor. The normal and tangential components of the drag force (F_D) generate thrust and negative torque on the rotor respectively. The cross section of a blade at an arbitrary radius (r) and a pitch angle (β) has been detailed in Figure 1-8. As the free stream velocity (U_∞) approaches the rotor due to the rotor angular velocity (ω), the relative wind velocity (U_{rel}) hits the rotor plane with a specific angle of incident (Φ) at each radius. Therefore, wind reaches each cross section with an angle that is called the angle of attack (i.e. the angle between the airfoil chord line and the relative wind direction (α)).

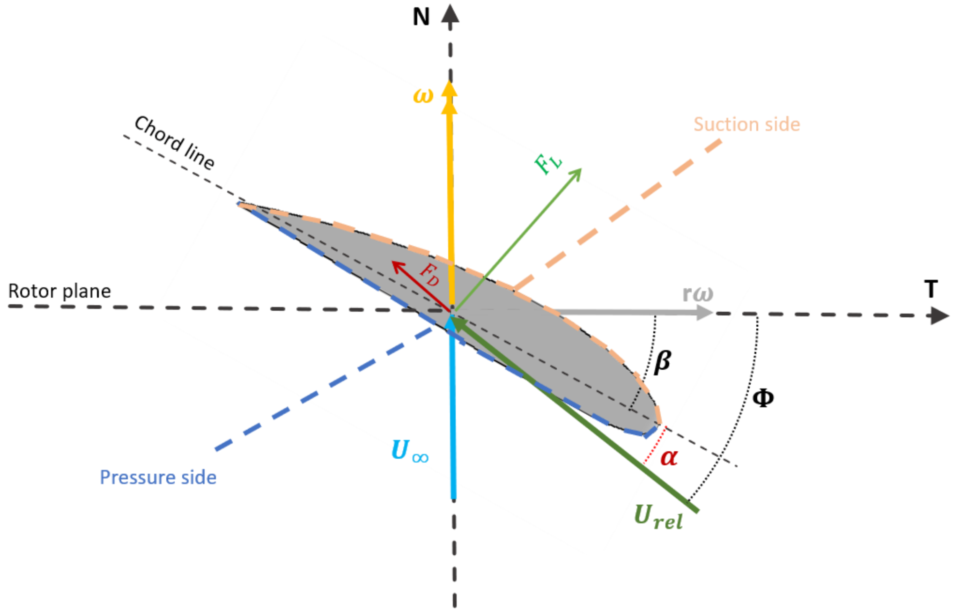

Figure 1-8: Blade element geometry, velocities and forces based on tangential (T) and normal (N) axes

Generating power based on lift enables these machines to move (rotate) at higher speeds compared to the incoming wind, unlike drag based turbines (e.g. Savinious wind turbine). In fact, the faster the point of optimum operating condition is, the more efficient the turbine will be. Based on third law of the motion, if the turbine generates its power mostly due to high rotational speed and relatively lower torques, it has higher efficiency. The less torque on rotor means less counteracting torque on the control volume of the air passing through the rotor and less wake flow rotation which essentially is wasted energy of the inflow. Therefore, an important design and operation parameter is the Tip Speed Ratio (TSR) which is the ratio of the tip speed of the blade and the free stream wind velocity. For a turbine with blade span of R and rotational speed of ω , the TSR is defined as:

$$TSR = \lambda = \frac{R\omega}{U_\infty}, \qquad \text{1-1}$$

The turbines with higher designed TSRs have more slender blades with less overall twist angles.

Turbine efficiency is defined by a power coefficient, which is the ratio of the converted power by the turbine to the total kinetic power of the flow as shown in equation 1-2.

$$C_p = \frac{P}{\frac{1}{2}\rho A {U_\infty}^3}, \tag{1-2}$$

P is the generated power, ρ is the density of the air and A is the sweeping area of the rotor. Theoretically, the efficiency by the Betz law [15] never exceeds ∼59%. This is calculated by writing the linear momentum and the Bernoulli equations upstream and downstream of the rotor. The main simplifying assumptions are: (I) homogeneous and incompressible steady flow; (II) rotor treated as a uniform actuator disk; (III) neglecting friction and flow rotation in the wake. The resulting equation indicates that if an ideal wind turbine were designed and operated such that the flow velocity at the rotor disc were 2/3 of the free stream velocity, then it would be operating at the point of maximum power output (i.e. Betz limit). More details are available in [15].

As the turbine operates, the pressure difference, on the two side of the blades, causes a leakage of the flow from the tip and root of the blades, which overall decrease the pressure difference and the power efficiency. These leakages due to sharp geometry of the root and tip are in the form of vortexes which then get advected downstream by the main flow in a helical pattern [15] due to wake rotation (Figure 1-9).

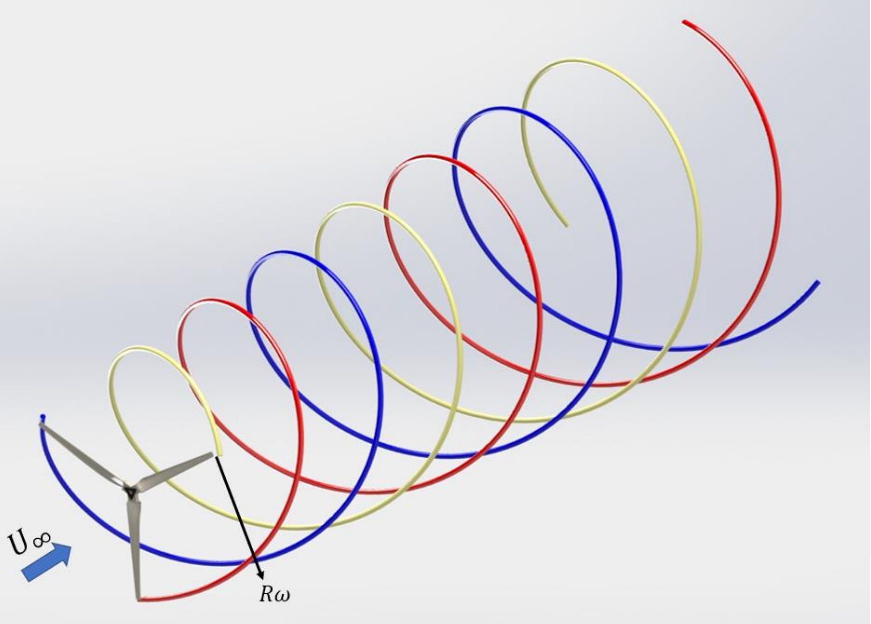

Figure 1-9: The blade tip vortex formation due to pressure difference on the pressure side and the suction side with their helical patterns in the near wake of an operating turbine

These helical vortex tubes can be advected up to 5 times the diameter of the rotor downstream depend on turbine’s operating TSR. The higher the TSR the sooner the vortices would break up and create a totally chaotic turbulent region at the wake. In the literature, this region with helical patterns is called near wake and the chaotic region is the far wake [16].

In this study, a model upwind, three-bladed 2.2 m diameter wind turbine and capable of producing 1kW rated power at 12 m/s is used for the experiments. It is the exact turbine that has been previously used for near wake [16] and the BEM (Blade Element Momentum) theory [17] studies. The net blade length is 0.91 m. The root and tip chord lengths are 12.7 cm and 5.4 cm respectively, and it has a linear chord distribution through the span. The chord and twist angle distributions along the blade span as well as the profile geometry of each section are shown in Figure 1-10. The profile type at each section of the blade is not provided by the manufacturer, but the airfoil presented here are the closest match.

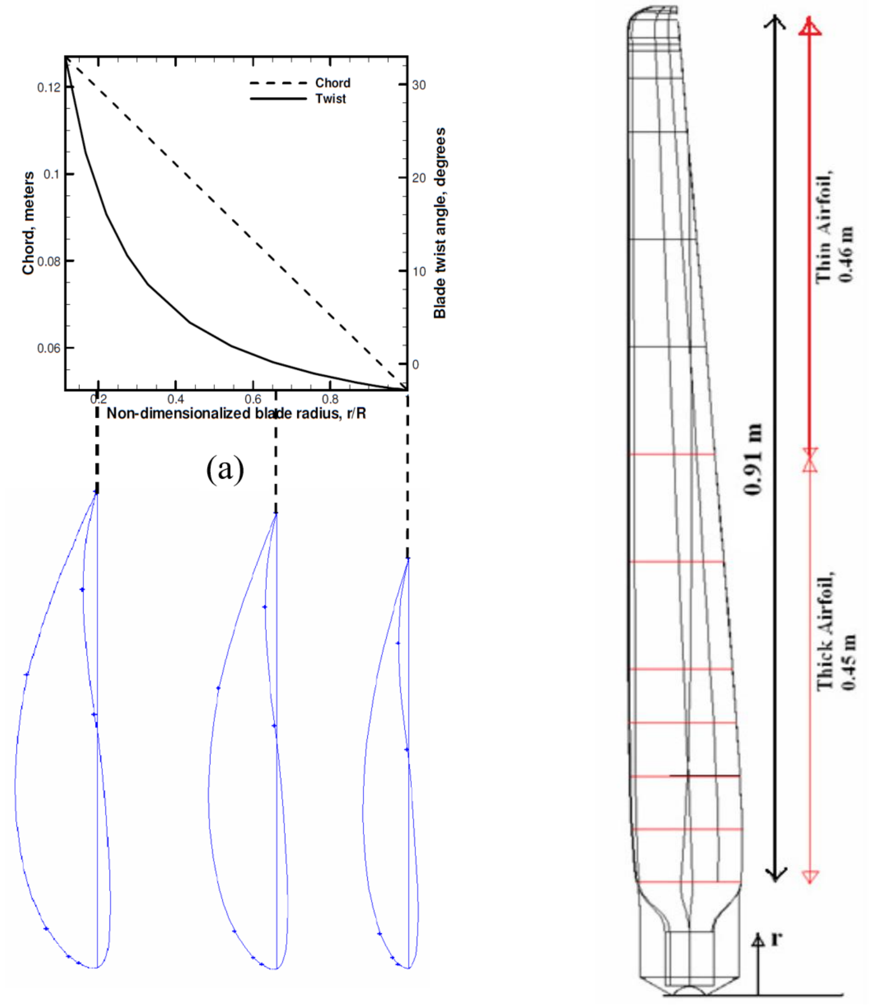

(a)

(b)

(c)

Figure 1-10: The geometry of the blade, (a) chord and twist distribution along the span, (b) the approximate airfoil geometry at each section and (c) blade shape, from [17]

To relate this study to full scale, a scaling method is proposed based on kinematic similarity (equation 1-3). Accordingly, the time that four complete tip vortex loops get advected in the wake by the free stream, is corresponded to the time that extreme conditions happen.

$$\frac{\boldsymbol{T_s} U_\infty \lambda}{2\pi R} = 4 \qquad \text{1-3}$$

Essentially, this assumption makes the scaled gust time ($\boldsymbol{T_s}$) function of operating TSR, free stream velocity, and the size (geometry) of the rotor. In current experiments, there is a large difference in Reynolds number compared to full scale, so the dynamic similitude has not been met. For more details about the scaling method please refer to section 2.2.4.

1.4 The IEC 61400-1 standard

As mentioned in section 1.2, to further decrease the LCOE of wind energy, these machines must have a long life span. Therefore, some guidelines and standards have been established for companies to increase the operational lifetime of these energy systems to at least 20 years. The Det Norske Veritas Germanischer Lloyd (DNV.GL) and International Electrotechnical Commission (IEC) have sets of standards commonly used for various design stand points. DNV GL mostly covers the various structural design aspects for offshore systems. Both have some deterministic design codes for commercial Horizontal Axis Wind Turbines (HAWT) in operating conditions with slight differences. The present research focuses on the IEC standard.

The IEC began working on the first international standard in 1988 for wind turbines, leading to the publication of IEC 61400. The first version of the Part 1 which includes the safety requirements of wind turbine generator systems was published at 1994 [18]. A revised edition containing some significant changes appeared in 1999 [19]. The third and forth edition came in 2005 [20] and 2019 [21]. In this research, the third edition of the IEC 61400-1 was considered due its deterministic approach to the definition of the extreme conditions which make physical development of their flow field in a lab environment more approachable. The standard covers various design aspects of turbines. Extreme operational conditions have been defined under “external conditions” category and are essentially dependent on the turbine’s class and size. All these extreme conditions have been simplified based on field measurements by attributing deterministic shape and duration for design purposes [22]. Details about the extreme operational condition mathematical models are presented in section 2.1.

1.5 Motivation and contribution

As it will be discussed in detail in Chapter 2, physical experimental studies of the transient events particularly the IEC extreme operational conditions are limited in literature. Developing a method to experimentally test the extreme conditions on scaled wind turbines is an important contribution to researchers in this field which can provide validation for numerical simulation of their effect on wind energy systems. Recently there have been some efforts for creating gust similar to the IEC using a sophisticated active grid [23]. However, the focus of their study was more on the mitigating the effect of gust on a wind turbine rather than the flow field itself without proposing a relevant scaling for the gust. In another study performed by Neunaber and Braud [24], a rotating blade (chopper mechanism) was utilized to make perturbation in the flow by blocking the cross section of the wind tunnel dynamically in time as it rotates. Using this setup, they were able to generate gusts in negative values. They proposed a scaling, based on which they needed to generate 1 s gusts, but their results show that the flow field does not recover to its initial stage. In addition, they were not able to generate uniform gust flow field as standard prescribes. They perform the experiment in a small wind tunnel section ($0.5 \times 0.5\ m^2$). Using the same method for generating gusts in larger and more practical wind tunnels will amplify the above-mentioned issues. The challenges that these studies had, motivated the current research work, which mainly propose (I) a relevant scaling method for extreme events applied for wind turbines; (II) experimentally reproducing scaled standardized extreme conditions. For this purpose, a set of 60 individually controlled fans at WindEEE Dome at Western University, Canada is utilized. The fan setups for creating the desired velocity fields, obtained by trial and error using a simplified CFD model of the test chamber. This work demonstrates the potential of this facility to generate generic extreme wind conditions which then can be applied to further investigate performance, loading and safety issues for HAWTs.

1.6 Thesis outline

This thesis includes three chapters additional to the Chapter 1. They are organized as follows. Chapter 2 has been formatted as the paper that was submitted to the journal of Wind Energy Sciences. It details the CFD studies in order to develop the numerical model of the flow field for the WindEEE test chamber. This CFD model was then used to obtain the fan setups prior to the experimental test campaign; this hybrid numerical/ experimental approach saved time in the experimental trial and error process of flow modulation to create the desired transient flow fields. This chapter also presents the results from experimental flow field measurements and their comparison with the predictions from the CFD and the IEC standard. Chapter 3 is also formatted as a paper which is submitted to the journal of Wind Energy Sciences. It experimentally examines the effect of the simulated extreme conditions on the loads and power performance of a scaled wind turbine. Chapter 4 summarizes the results and provides direction and comments for future work.

1.7 References

[1] G. T. Pecl G. T. Pecl, M. B. Araujo, J. D. Bell, J. Blanchard, T. C. Bonebrake, I-Ching Chen, T. D. Clark, R. K. Colwell, F. Danielsen, B. Evengard, L. Falconi, S. Ferrier, S. Frusher, A. Garcia, R. B. Griffis, J. Hobday, C. Janion-Scheepers, M. A. Jarzyna, S. Jennings, J. Lenoir, H. I. Linnetved, V. Y. Martin, P. C. McCormack, J. McDonald, N. J. Mitchell,T. Mustonen, J. M. Pandolfi, N. Pettorelli, E. Popova, S. A. Robinson, B. R. Scheffers, J. D. Shaw, J. B. Sorte37, J. M. Strugnell, J. M. Sunday, Mao-Ning Tuanmu, A. Verges, C. Villanueva,T. Wernberg, E. Wapstra, and S. E. Williams, “Biodiversity redistribution under climate change: Impacts on ecosystems and human well-being,” *Science*, vol. 355, no. 6332, p. eaai9214, Mar. 2017, doi: 10.1126/science.aai9214.

[2] R. M. Key, A. Kozyr, C. L. Sabine, K. Lee, R. Wanninkhof, J. L. Bullister, R. A. Feely, F. J. Millero, C. Mordy, and T. Peng, “A global ocean carbon climatology: Results from Global Data Analysis Project (GLODAP),” *Global Biogeochemical*

Cycles, vol. 18, no. 4, 2004, doi: 10.1029/2004GB002247.

[3] R. Munang, I. Thiaw, K. Alverson, J. Liu, and Z. Han, “The role of ecosystem services in climate change adaptation and disaster risk reduction,” *Current Opinion in Environmental Sustainability*, vol. 5, no. 1, pp. 47–52, 2013, doi: https://doi.org/10.1016/j.cosust.2013.02.002.

[4] D. Lüthi, M. Le Floch, B. Bereiter, T. Blunier, Jean-Marc Barnola, Urs Siegenthaler, D. Raynaud, J. Jouzel, H. Fischer, K. Kawamura, and & T. F. Stocker, “High-resolution carbon dioxide concentration record 650,000–800,000 years before present,” *Nature*, vol. 453, no. 7193, pp. 379–382, 2008, doi: 10.1038/nature06949.

[5] “Graphic: The relentless rise of carbon dioxide – Climate Change: Vital Signs of the Planet.” https://climate.nasa.gov/climate_resources/24/graphic-the-relentless-rise-of-carbon-dioxide/ (accessed Sep. 10, 2020).

[6] D. T. Shindell, B. P. Walter, and G. Faluvegi, “Impacts of climate change on methane emissions from wetlands,” *Geophysical Research Letters*, vol. 31, no. 21, Nov. 2004, doi: 10.1029/2004GL021009.

[7] G. Gunkel, “Hydropower - A green energy? Tropical reservoirs and greenhouse gas emissions,” *Clean - Soil, Air, Water*, vol. 37, no. 9, pp. 726–734, Sep. 2009, doi: 10.1002/clen.200900062.

[8] B. Singh and J. Sharma, “A review on distributed generation planning,” *Renewable and Sustainable Energy Reviews*, vol. 76. Elsevier Ltd, pp. 529–544, Sep. 01, 2017, doi: 10.1016/j.rser.2017.03.034.

[9] “U.S. Energy Information Administration (EIA).” https://www.eia.gov/ (accessed Apr. 11, 2020).

[10] “Global Map - Wind Atlas - Environment and Climate Change Canada.” http://www.windatlas.ca/maps-en.php (accessed Apr. 11, 2020).

[11] “Installed Capacity - Canadian Wind Energy Association.” https://canwea.ca/wind-energy/installed-capacity/ (accessed Apr. 11, 2020).

[12] M. Ragheb, “Economics of Wind Power Generation,” in *Wind Energy Engineering: A Handbook for Onshore and Offshore Wind Turbines*, Elsevier Inc., 2017, pp. 537–555.

[13] “Renewable Power Generation Costs in 2018,” */publications/2019/May/Renewable-power-generation-costs-in-2018*.

[14] M. O. Hansen, *Aerodynamics of wind turbines*, Third ed. Abingdon, UK: Routledge, 2015.

[15] M. Hansen, *Aerodynamics of wind turbines*. 2015.

[16] P. Hashemi Tari, K. Siddiqui, and H. Hangan, “Flow characterization in the near-wake region of a horizontal axis wind turbine,” *Wind Energy*, vol. 19, no. 7, pp. 1249–1267, Jul. 2016, doi: 10.1002/we.1895.

[17] M. Refan and H. Hangan, “Aerodynamic performance of a small horizontal axis wind turbine,” *Journal of Solar Energy Engineering, Transactions of the ASME*, vol. 134, no. 2, 2012, doi: 10.1115/1.4005751.

[18] “IEC 61400-1, Wind energy generation systems - Part 1: Design requirements, 1994.”

[19] “IEC 61400-1. Wind turbine generator systems ; Second edition- 1999.”

[20] “IEC 61400-1. Wind turbine generator systems ; Third edition- 2005.”

[21] “IEC 61400-1. Wind turbine generation systems ; Forth edition- 2019.”

[22] P. Cheng and W. Bierbooms, “Extreme gust loading for wind turbines during operation,” Jan. 2001, doi: 10.2514/6.2001-45.

[23] V. Petrović, F. Berger, L. Neuhaus, M. Hölling, and M. Kühn, “Wind tunnel setup

for experimental validation of wind turbine control concepts under tailor-made reproducible wind conditions," in *Journal of Physics: Conference Series,* 2019, vol. 1222, no. 1, doi: 10.1088/1742-6596/1222/1/012013.

[24] I. Neunaber and C. Braud, "First characterization of a new perturbation system for gust generation: the chopper," *Wind Energy Science,* vol. 5, no. 2, pp. 759–773, Jun. 2020, doi: 10.5194/wes-5-759-2020.

Chapter 2

2 Numerical and experimental simulation of extreme operational conditions for horizontal axis wind turbines based on the IEC standard ©

In this study, the possibility of simulating some transient and deterministic extreme operational conditions for horizontal axis wind turbines based on the IEC 61400-1 standard using 60 individually controlled fans in the Wind Engineering, Energy and Environment (WindEEE) Dome at Western University was investigated. Experiments were carried out for the Extreme Operational Gust (EOG), positive and negative Extreme Vertical Shear (EVS), and Extreme Horizontal Shear (EHS) cases, tailored for a scaled 2.2 m horizontal axis wind turbine. For this purpose, firstly a numerical model for the test chamber was developed and used to obtain the fans' configurations for simulating each extreme condition with appropriate scaling prior to the physical experiments. The results show the capability of using numerical modeling to predict the fans' setup based on which physical simulations can generate IEC extreme conditions in the range of interest.

2.1 Introduction

Wind energy is one of the primary sources of renewable energy for mitigation of the increasing global energy demand. However, one of the basic factors for this market to thrive is a continued reduction of the levelized cost of electricity (LCOE), which is enhanced by ensuring the life time of the wind energy systems is reliably long [1]. Having a long life cycle for these energy systems dramatically increases the probability of them encountering various extreme weather and wind conditions. Therefore, the design of wind

---

© This chapter has been submitted to the to the journal of Wind Energy Sciences, under co-authorship of K. Shirzadeh, H. Hangan and C. Crawford energy systems must consider extreme environmental conditions with statistically accurate return periods. The International Electrotechnical Commission (IEC) has some deterministic design codes for commercial Horizontal Axis Wind Turbines (HAWT) in operating conditions, specifically in the third edition of the IEC 61400 part one [2]. These extreme models are relatively simple and are not able to capture the true coherent turbulent wind characteristics [3]–[5]. This is especially true in complex terrain where the gust time evolution profiles are highly asymmetric and non-Gaussian [6]. It has also motivated the most recent edition of the IEC standard [7] to utilize statistical methods for characterizing extreme gust event performance and extrapolation of load cases. This has been enabled by computational resources to analyse wind energy systems in dynamic wind environments to expand their external condition models. However, the third edition of the IEC standards was used in the work presented here as an initial step towards gust experimentation and represents an incremental development of a gust loading experimental capability. Progressing to a stochastic experimental approach, is left for future work and will be very challenging.

One of the extreme cases in the standard is the extreme operational gust (EOG). A gust is defined as a sudden increase in velocity over its mean value, which is a transient feature of a turbulent wind field [8].These turbulent features in the Atmospheric Boundary Layer (ABL) depend on topography, surface roughness, up-stream obstacles, thermal stability [9] and mesoscale climactic systems such as thunderstorms and downbursts [10]. In theory, for different applications, there are various simplified models of gust based on a peak factor and the whole rising and falling time in the wind speed. The peak factor is the ratio of the peak velocity (maximum or minimum) and the average wind speed. Wind gusts can happen over various length and time scales in nature. The most damaging gusts for any type of structures are the ones that have the same length scale as the structure that can envelope the whole structure [6]. Smaller gusts, relative to wind turbine size can induce dynamic stall and the gust slicing effect (i.e. recurring high loads as the blade slices through the spatial/temporal gust region several times). The wind gusts also can cause intermittencies in the power output of wind turbine generators. For a small electricity network, these fluctuations in power generation can cause serious problems (e.g. unstable grid voltage and frequency) for managing power transmission and distribution [11], [12]. The worst case in both terms of the grid stability and the loading on the turbine is when the gust peak speed is higher than the wind turbine cut-out speed (i.e. a specific speed that turbine comes to complete parked position for safety reasons, usually about 25 m/s), which, if prolonged enough can cause the control system to abruptly stop the wind turbine [13]. From an aerodynamic point of view, gusts can result in undesired acceleration of the rotor and drivetrain.

The most reasonable solution is usually an adjustable generator load or blade pitch angles after detection of the gust for modern wind turbines [14], [15]. Developing LIDAR technology can make a substantial contribution in controlling the wind turbine by measuring the wind field upstream, thereby giving enough time for the control system to react properly [16], [17].

In addition to uniform gusts, the standard specifies deterministic Extreme Vertical and Horizontal Shears (EVS, EHS). These Extreme Wind Shears (EWS) can induce asymmetric loads on the rotor which are in turn transferred into the whole structure. The vertical shears can induce tilting or out-of-plane moments on the rotor and nacelle [18]. In a positive vertical shear, the blade moving at higher height could experience stall while the one moving at lower height will experience a reduction in overall angle of attack relative to design condition (and vice versa for negative vertical shear) [19]. If the shear is extreme enough, the blades may experience a phenomenon known as dynamic stall [20], [21]. All these phenomena together will result in high fluctuations in power generation, as well as highly dynamic fatigue loads on the structure [22], [23]. The effects of horizontal shear are similar to vertical shear in terms of power performance and blade fatigue loads. However, EHS also induces yaw moments. These transient shears can happen for similar reasons as uniform gusts, but mostly happen within wind farms, where the downstream wind turbines are partially exposed to the wakes of other operating turbines [24], [25].

The IEC defines a classification for commercial wind turbines based on a reference wind speed and turbulence intensity, in a way that covers most on-shore applications [2]. The Turbulence Intensity (TI) is defined as the ratio of the standard deviation of wind speed fluctuations to the average wind speed both calculated in 10 min intervals. TI levels of

16%, 14% and 12% corresponded to the A, B and C reference turbulence classes (I_{ref}). For velocity references (U_{ref}), 3 classes have been defined (I, II, III) with 50, 42.5, 37.5 m/s as reference wind speeds, with one further class for special conditions (e.g. offshore and tropical storms) which should be specified by the designer. These reference velocities are used to calculate parameters related to the turbine external conditions. For example, the standard mean value of the wind speed over a 10 min interval based on the turbine class is 0.2 U_{ref}. An extreme wind speed model as a function of height (Z), with respect to the hub height (Z_{hub}) with recurrence periods of 50 years (U_{e50}) and 1 year (U_{e1}), is defined as follows:

$$\begin{aligned} U_{e50}(z) &= 1.4U_{ref}\left(\frac{Z}{Z_{hub}}\right)^{0.11} \\ U_{e1}(z) &= 0.8U_{e50}(z) \end{aligned} \qquad \text{2-1}$$

This definition is used for calculating the gust magnitude of the EOG.

The design stream-wise turbulence standard deviation (σ_u) is defined by a normal turbulence model:

$$\sigma_u = I_{ref}(0.75U_{hub} + b); \quad b = 5.6\ \frac{m}{s}, \qquad \text{2-2}$$

U_{hub} is the average wind velocity at the at hub-height and b is a constant. Accordingly, the hub height gust magnitude (U_{gust}) is given as:

$$U_{gust} = min\left\{1.35(U_{e1} - U_{hub}); 3.3(\frac{\sigma_u}{1 + 0.1\left(\frac{D}{\Lambda_u}\right)})\right\} \qquad \text{2-3}$$

Considering t as the instantaneous time and $t = 0$ at the beginning of the gust, the uniform EOG as function of time is defined as:

$$U(t) = \begin{cases} \overline{U_{hub}} - 0.37U_{gust}\, sin\frac{3\pi t}{T}\left(1 - cos\frac{2\pi t}{T}\right); when \quad 0 \le t \le T, \\ \overline{U_{hub}}; \quad when\, t > T\ or\ t < 0, \end{cases} \qquad \text{2-4}$$

T is the duration of the gust, specified as 10.5 seconds. D is the diameter of the rotor, and Λ_u is the longitudinal turbulence scale parameter which is a function of the hub height:

$$\Lambda_u = \begin{cases} 0.7Z_{hub} & for\ Z_{hub} \leq 60\ m, \\ 42m & for\ Z_{hub} > 60\ m, \end{cases} \qquad 2\text{-}5$$

The EVS and EHS have similar equations and both considered as EWS, which can be added to or subtracted from the main uniform or ABL inflow. The EVS as function of height (Z) and time can be calculated using the:

$$U_{EVS}(Z,t) = \begin{cases} \left(\frac{Z - Z_{hub}}{D}\right)\left(2.5 + 0.2\,\beta\sigma_u\left(\frac{D}{\Lambda_u}\right)^{0.25}\right)\left(1 - cos\left(\frac{2\pi t}{T}\right)\right); when\quad 0 \leq t \leq T, \\ 0\quad ;\ when\ t > T\ or\ t < 0, \end{cases} \qquad 2\text{-}6$$

β is a constant with value of 6.4 and T is 12 s in the EWS. The peak factor of the EOG decreases with increasing size of the turbine or decreasing hub height, and vice versa for the EWS based on these equations.

Along with more common steady state experiments [26], [27], developing transitory flow field experiments have attracted the interests of researchers during the past few decades [28], [29] to evaluate the various computational techniques or to directly investigate complex phenomena in different applications. In the wind energy field some efforts have been made to produce gusts; for example, using active grids [30], [31] and a chopper mechanism [32]. Developing these unsteady flow fields basically comes down to the experiment targets and the available wind tunnel facilities. In this study, the generation of the EOG and the EWSs unsteady flow fields with relevant scaling (customised for a 2.2 m scaled HAWT) using 60 individually controlled jet fans in the WindEEE dome are considered. This work presents a new numerical model of the WindEEE dome test chamber which can be used to predict fan settings for any custom steady or unsteady 2D flow fields before the physical experiment, and the capability of this facility to physically generate the gusts and shears similar to IEC standard during experiments. The focus of this paper is just on the time evolution of the simulated extreme conditions' flow fields which is a prologue for future experiments including an actual HAWT model.

This chapter is organized in three sections beside the introduction and it is as follows. Section 2.2 details the development of the numerical model for the WindEEE test chamber which was used to obtain the fan setups to use in physical simulation of the gusts. This section also provides a length and time scaling of the gust which based on that the target gusts for experimental campaign are introduced. Section 2.3 presents the results from velocity measurements at the test section in two parts, firstly the steady shears to assess the accuracy of the developed numerical model to simulate the shear layers and secondly the final transient simulated gusts and their comparison with IEC standard. Section 2.4 provides some conclusions.

2.2 Methodology

2.2.1 WindEEE dome

The physical experiments were conducted in the WindEEE Dome at Western University, Canada. This is a versatile facility that can be run at different modes for creating various non-stationary wind systems [33]. It has an inner test chamber with a 25 m diameter hexagonal footprint and 3.8 m height. It has a total 106 fans, including 60 fans installed on one wall and 40 fans over the other five peripheral walls. There are also 6 larger fans in a plenum above the test chamber which are mostly used for generating 3D flows like tornados and downbursts. The test chamber is in turn surrounded by an outer shell. The dome inner shell/test chamber along with outline of the outer shell with the flow path in the closed-circuit 2D flow mode (e.g. ABL, shear flows and etc) are presented in Figure 2-1a. In 2D flow mode, the louvers at the top and peripheral sides of the test chamber are closed and the flow is energized only by the 60 fans, then it reaches to the test section (center of the test chamber) and then exits the test chamber through the mesh of the wall at the opposite end, then recirculating over the top while passing through the heat exchangers, and finally back to the 60 fans' inlet. Each fan is 0.8 m in diameter with 30 kW nominal maximum power. In order to reach higher velocities and better flow uniformity characteristics at the center of the test chamber, a two-dimensional contraction can be setup to streamline the flow as shown in Figure 2-1b.

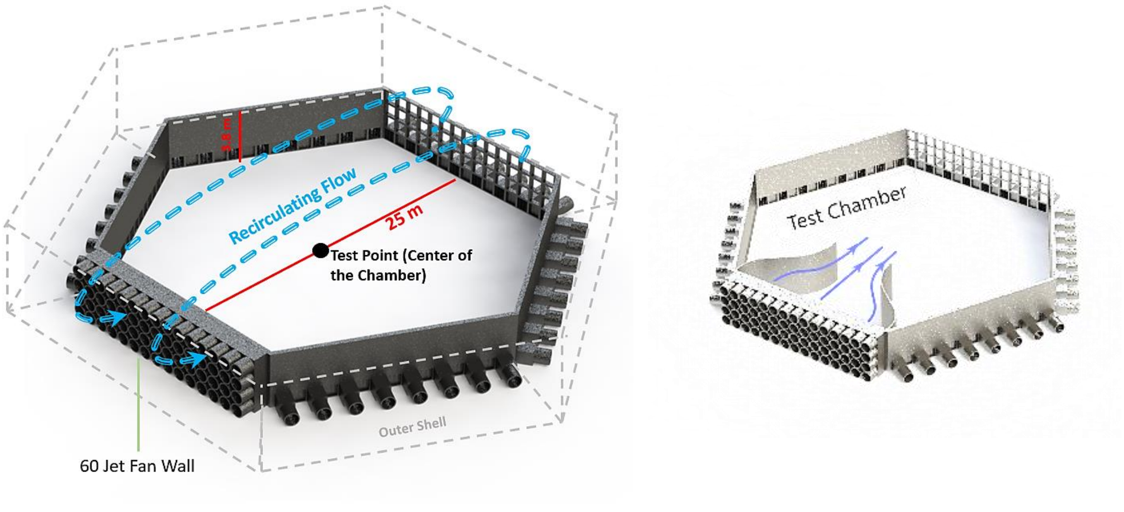

(a) (b)

Figure 2-1. A brief geometry of the WindEEE dome, (a) the test chamber with outline of the outer shell along with the flow path in closed-circuit 2D flow mode, (b) the test chamber with contraction walls

The power set-points of the 60 fans can be adjusted by the software as fast as 2Hz. However, this does not imply the fans themselves can throttle from 0% to 100% power at 2 Hz (due to rotational inertia of the fans' rotors and electrical current filtering it takes ~3 s for the fans to adjust).

Another feature are the fans with adjustable inlet guide vanes which can regulate the amount of flow rate through the fans. These vanes can be adjusted uniformly from 0% open (close) to 100% open (Figure 2-2). They can also be adjusted dynamically by setting an actuation frequency, duty cycle and an initial position. The actuation frequency specifies the time between two cycles, while the duty cycle specifies the duration of an individual cycle specified as a percentage of the time between two successive cycles. All these features allow the generation customizable dynamic flows.


(a) (b)

Figure 2-2. The adjustable vanes at the inlets of the 60 fans wall, (a) 100% open vanes, (b) 70% open vanes

2.2.2 Numerical flow analysis setup and tuning/ validation

In order to have a better understanding of the flow field in the test chamber, a numerical model for the test chamber was created using the commercial Star-CCM+ CFD software, which helped to predict the fan power setups for different scenarios prior running the experiments.

For this purpose, four simplified symmetrical domains of the test chamber were generated to save considerable CPU time as listed at Table 2-1. As this table outlines, the domains V and V-c were used for simulating EOG, EVS and ABL flows; domains H and H-c were used for simulating EHS.

Table 2-1: The symmetrical domains of the test chamber used for simulating different cases

Picture of the Domain	Application	Domain ID
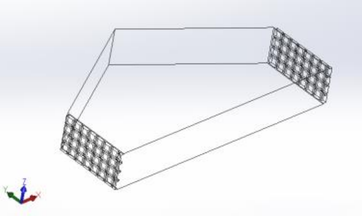	Simulating ABLs and EVS & EOG and tuning the boundary conditions parameters	V
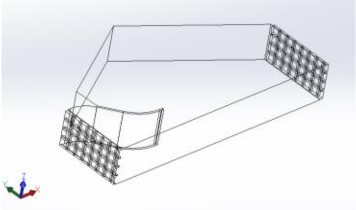	Simulating ABLs and EVS & EOG with contraction walls and tuning the boundary conditions parameters	V-c

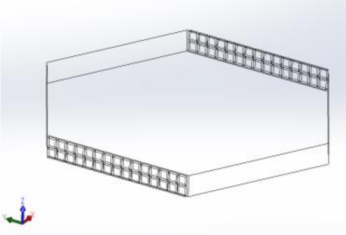	Simulating EHS	H
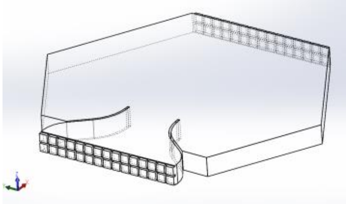	Simulating EHS with contraction walls	H-c

In order to discretize the domains, three mesh setups (M1, M2 and M3) were considered for the polyhedral automated mesh function, built-in Star-CCM+ software. The general details for the generated grids are presented in Table 2-2. For all the cases, 5 prism layers with a total thickness of 0.05 m and with stretching of 30 % at the solid walls with minimum of 4 elements in the gaps were used; the surface curvature and surface growth rate were left at their default values (6 degrees and 20% respectively) with no specified mesh density in the domains. In addition, in domains with contraction walls a custom control refinement on the surfaces of the contraction walls was used to create elements half of the general base size. The fans were modelled as squares with individual velocity inlet boundary conditions. The outflow grid on the opposite wall was treated as uniform pressure outlet. All other surfaces were treated as no-slip walls. Due to broad range of the Reynolds number across the domain, controlling the wall y+ was challenging. Therefore, for modelling the Reynolds stresses in the RANS equations, two-layer K-epsilon (k-ε) turbulence model was chosen.

The next step was to calibrate the boundary condition parameters based on the previous experiment data that were available for scaled ESDU ABL profiles both with and without contraction walls [34]. The simulated fan powers were then adjusted to reach the desired average velocity profiles at the test section to match the existing experimental data. The M1 setup at domain V and V-c were used for preliminary tuning of the input values at the inlets and the outlet boundary condition parameters in order to get the best match with the available data at the test section. The best results corresponded to an inlet turbulence intensity of 8% with length scale of 0.2 m and the outlet boundary set as a pressure outlet with uniform zero-gauge pressure, 1% turbulence intensity and 0.05m length scale. Working at full power, the fans can generate 13 and 31 m/s of uniform wind velocity at the test section without and with contracting walls respectively. At the end the simulation results showed that the full fan powers corresponded to a 16.5 m/s inlet boundary velocity. The fan power set-points were then simplified as a linear interpolation between 0 and 16.5 m/s for the velocity inlets.

Table 2-2: Detail of grid sizes for each domain

Grid name tag	M1	M2	M3
Number of Cells for Domain V (Million)	**1.41**	**2.53**	**5.52**
Number of Cells for Domain V-c (Million)	**2.37**	**3.72**	**6.75**
Number of Cells for Domain H (Million)	**N/A**	**1.93**	**N/A**
Number of Cells for Domain H-c (Million)	**N/A**	**3.00**	**N/A**
Base size (m)	**0.1**	**0.08**	**0.06**

The mesh independency check was defined by the incrementally refined grids M1 to M3 using the velocity profiles at the test section for the ABL profiles which have different fan power set points for each row (Figure 2-3). For low speed setup (without contraction) they were at 50, 70, 70 and 50% from bottom row to top (Figure 2-3a); for the setup with contractions, the fans are at 50, 65, 75 and 75% (Figure 2-3b); The velocity profiles from the CFD results was defined by a probe line with 40 points over the entire height of the chamber.

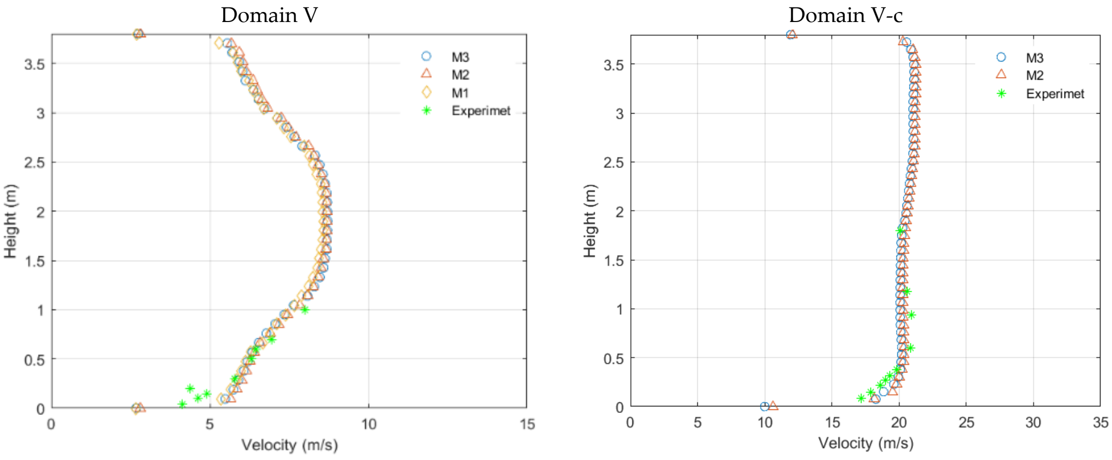

(a) (b)

Figure 2-3. The mean ABL velocity profiles at the test section for different mesh setups comparing with the experimental data [34], (a) low speed (without contraction) and (b) high speed (with contraction) mean velocity vertical profiles

According to Figure 2-4a &b showing the relative errors between velocities at each height; the largest disconformities between different mesh setups occur close to the wall which for this research is not the most important region. The more critical region for the present experiments is at the middle heights where the wind turbine rotor will be located. That being said, even the M1 setup has an acceptable range of error (~1%) at mid-height. However, the M2 mesh setup was chosen as the best compromise of computation speed and accuracy.

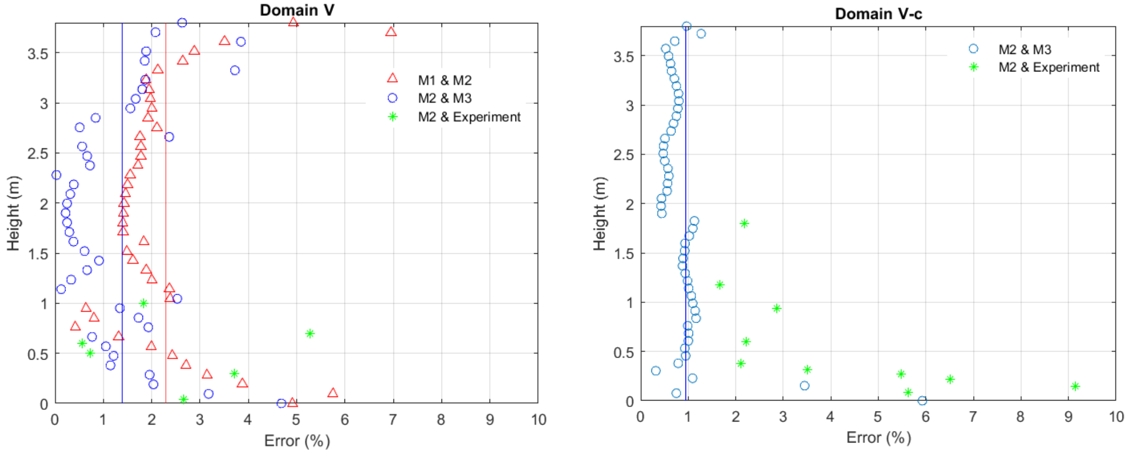

(a) (b)

Figure 2-4. The relative errors for (a) low speed velocities and (b) high speed velocities, the solid lines are the mean value for the errors over the whole height

The discrepancy between the CFD simulation (M2) and the experimental data also increases close to the wall. This error is rooted in uncertainty of the implemented turbulence model and relative course mesh size close to the wall in the numerical model. Nevertheless, they are in an acceptable range of engineering applications (under 10% of relative error). A picture of discretized domain V-c with the M2 grid is shown in Figure 2-5.

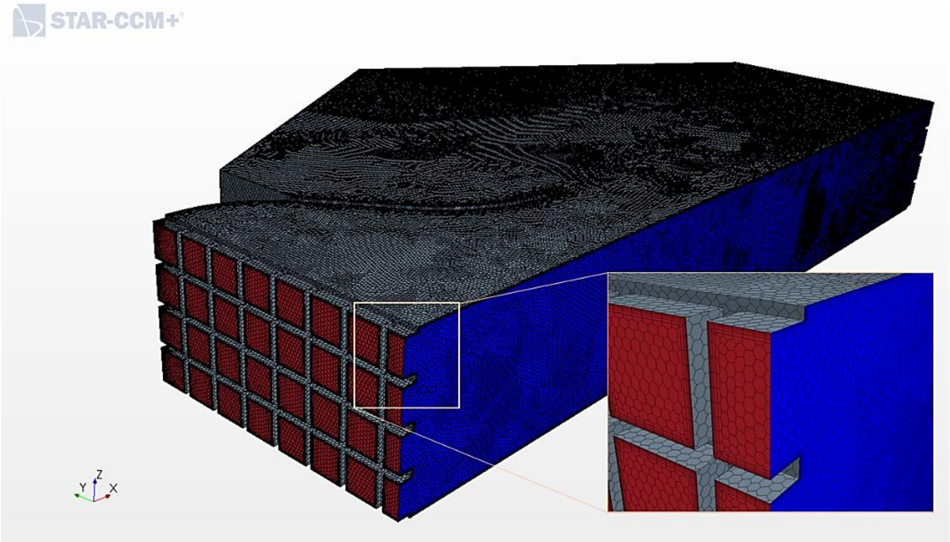

Figure 2-5. The M2 grid for the V-c domain

As described, this numerical model has been developed based on a set of steady ABL experimental data. The first application of it was to generate a calibration table that related the steady fan power set-points to the mean velocity magnitudes and profiles at the test section. This table was used to predict the fans' powers in generating the EOG. For simulating the EWSs, only the peak stages of these extreme events were considered for modelling, again in steady condition in order to obtain the fan setups at the peak of the corresponding wind shear event (see 2.3.1). These numerical simulations neglect the closed loop flow recirculation dynamics in the dome. Nevertheless, it produces a reasonable prediction of the fan setups for a specific flow field in a reasonable amount of time.

2.2.3 Experimental setup for velocity measurements

The velocity measurements were obtained with seven cobra probes. These robust probes [35] are capable of measuring the incoming airflow velocity within a cone shape of 45° with up to 10 kHz sampling frequency. Each probe has 4 pressure tabs at the head (0.5mm each) and is able to measure three velocity components with measuring range from 2 to 45 m/s with $\pm$0.5 m/s, and $\pm$1° pitch and yaw accuracy up to approximately 30 % turbulence intensity. In this study, the average stream wise wind velocity was 5 m/s; therefore, all the presented wind measurements have $\sim$ 10% accuracy in average.

Two different setups for velocity measurements were used; vertical and horizontal arrangements (Figure 2-6a & b). The sampling duration was 60 s with sampling frequency of 2000 Hz for each measurement run. The sampling duration was considered long enough compared to the 5 s extreme events to check for any unexpected perturbation in the flow field due to running the experiments in closed loop mode as the flow recirculates, by considering the flow recalculation path (~25+4+25+4=58 m) and the average wind speed (~5 m/s) which give recirculation time of 12 second. The precise turbulence characteristics is not the major objective of the current study, so the sampling frequency was chosen based on previous studies in this facility [36], [37]. In each extreme event multiple actuation times for modulating either the fan powers or the IGVs were considered; this study presents the best results compared to the target extreme events from an individual test run. More detail about cobra probes connection is presented in Figure 2-6d (just one of the probes is presented in this figure). The blue and yellow arrows are used for annotation of connections and equipment respectively. For correct measurements these probes need a static reference pressure. Therefore, all of them were connected to the static pressure side of a pitot tube via a manifold. The pitot tube was installed close to the cobra probe E in the middle of the array. Each cobra probe interface box has four cobra probe and eight analog input channels (the analog channels were not used). Therefore, two interface boxes were used which were connected with a specific synchronizing cable. Then each of these boxes were connected to the same A/D card via USB cables. The A/D card then was connected to a laptop that had the required TFI software installed.

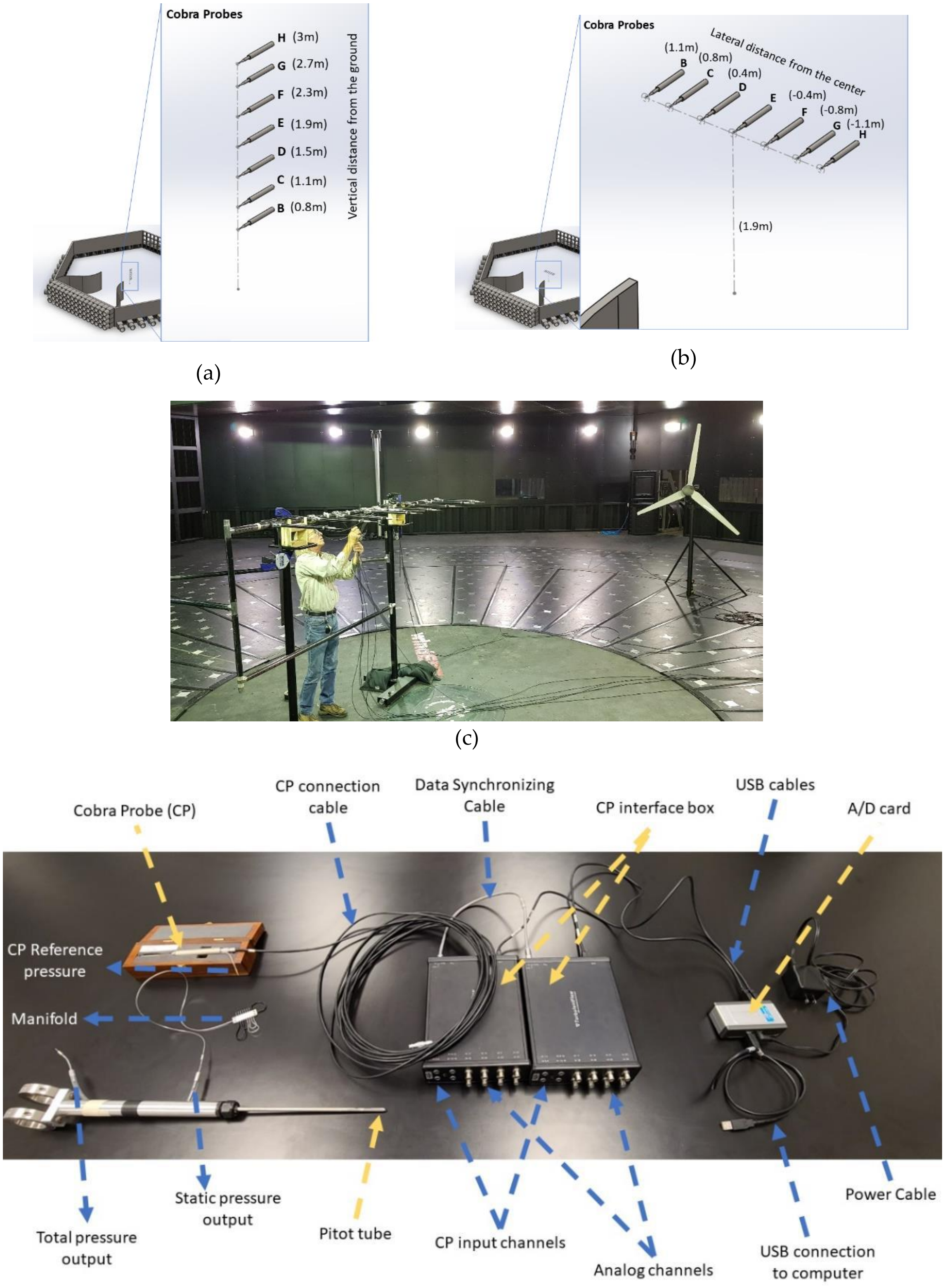

(a)

(b)

(c)

(d)

Figure 2-6. The arrangement of cobra probes based on the dimension of a 2.2m diameter HAWT for (a) vertical and (b) horizontal measurements at the center of the test section, (c)

Setting up the 7 cobra probes in a horizontal arrangement at the test section, (d) Cobra probe connection details

The locations of the probes were chosen based on the dimension of the available wind turbine in the facility. This turbine has a 2.2 m diameter with adjustable hub height, chosen as 1.9 m [38]. This entire paper is dedicated just to the development of the flow field. Investigation the effect of these unsteady wind conditions on the turbine is left for future work.

2.2.4 Gust length and time scaling

The time durations of the extreme events (T), as mentioned earlier, are 10.5 s for EOG and 12 s for EWS [2]. Subsequently, the gust durations correspond to 3 to 4 complete rotor revolutions periods for full-scale turbines (which usually have angular speed of 15-18 RPM in 10 m/s average wind speed). Usually, for a scaled wind turbine in the wind tunnel 4 rotor revolutions happen on the order of a second at the nominal operating condition. This gust time scale would be impossible to simulate at WindEEE facility given the physical limitations of the hardware. Therefore, by assuming that the time scale of the gust is equal to propagation time of 4 loops of a blade tip vortex downstream in the wake. The relevant gust time becomes function of turbine operating parameters and wind speed which then can be adjusted. We can calculate the propagation length and time of these vortex loops based on the definition of the Tip Speed Ratio (TSR:$\frac{blade\ tip\ speed}{free\ stream\ speed}$); assuming a uniform wake we have:

$$\Omega = \frac{\lambda U_{hub}}{R}\,[rad/s],$$

$$\Omega' = \frac{\lambda U_{hub}}{R} \times \frac{1}{2\pi}\,[rev/s], \qquad \text{2-7}$$

$$U_{hub} \times \frac{1}{\Omega'} = \frac{2\pi R}{\lambda}\left[\frac{m}{rev}\right],$$

where Ω is the angular velocity in radiant per second and $\Omega'$is in revolution per second, λ is TSR and R is the radius of the rotor; with some rearrangement the last part in equation 2-7 can be rewritten as follow:

$$\frac{L'}{D} = \frac{T'U_{hub}}{D} = \frac{\pi}{\lambda}, \tag{2-8}$$

the $L'$and T' are the length and time duration for propagation of one vortex loop in the wake. Based on the equation 2-8 and our assumption, an appropriate gust time and length can be calculated from:

$$\frac{\boldsymbol{L_s}}{D} = \frac{\boldsymbol{T_s}U_{hub}}{D} = 4\frac{\pi}{\lambda}, \tag{2-9}$$

Accordingly, the scaled time duration (T_s) is function of TSR, free stream velocity and the diameter of the rotor. The scaled length (L_s) is function of TSR and diameter of the rotor (Figure 2-7).

If the scaled turbine works at the same TSR and free stream velocity as the full-scale commercial HAWT, the time and length scale would be equal to their geometrical scale (i.e. the ratio of diameters).

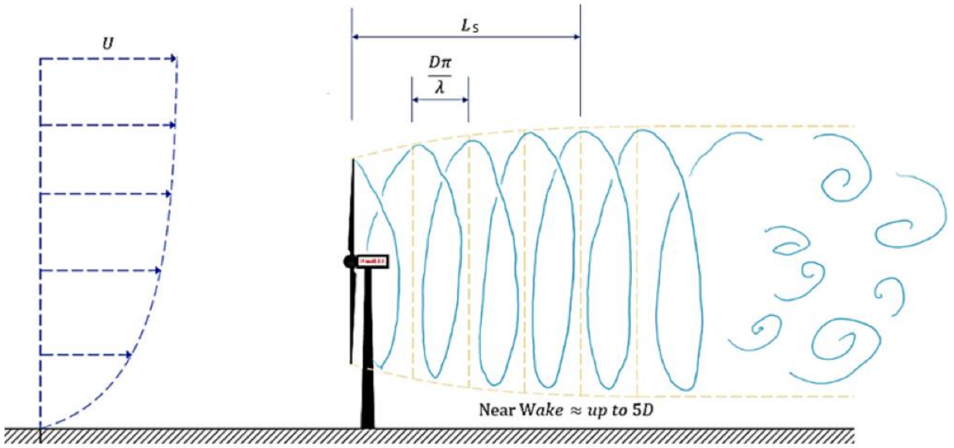

Figure 2-7. Visual representation of the length and the time scale proper for the extreme conditions with assuming a symmetric wake

The flow behaviour in the near wake region is directly correlated to the overall performance of a HAWT. Matching the time duration of the extreme condition to the propagation of 4 vortex loops in the wake should be a reasonable comparison to the full scale in terms of variation of power and loads on the wind turbine.

For a commercial B-III class HAWT with 92 m diameter rotor and 80 m hub height, at 10 m/s average velocity, the prescribed EOG and EVS are presented in Figure 2-8a & b. The time windows in these figures start and end with the extreme events.

The physical experiments showed that the fastest possible gust events with the required peak factor were around 5 seconds due to the hardware limitation. Therefore, to match the extreme event period to the suggested scaling assumptions, the 2.2 m scaled wind turbine should work in 5 m/s free stream velocity with operating TSR of 1.1, then it would take 5 seconds for the four complete loops of the tip vortexes generated by a specific blade to propagate in the wake. Accordingly, in all of the simulations and experiments the hub height velocity was kept at 5 m/s. Assuming a similar B-III class for the scaled HAWT with the hub height of 2 m, the scaled extreme condition profiles are shown in Figure 2-8c & d; in the scaled EOG velocity should uniformly rise from 5 to ~7.8 and then back to 5 m/s in 5 seconds with ~1 m/s drops before and after the main peak relative to the average free stream velocity (Figure 2-8c). However, in the experiments the gusts have been simplified by not including the velocity drops (the red dashed-line in Figure 2-8c). This simplification stretches the actual rising and falling time from ~ 2.5 to 5 s. Yet, this is the compromise that was made due to the hardware limitations. Hence, in this study, the target EOG has the same falling and rising time period as the scaled EWSs. The pre-post dips in the standard EOG reflect field data wherein gusts are preceded by lulls; however for the purpose of investigating peak loading during gust events, for a machine nominally operating at the mean wind speed and assumed not responding much during the lull period, it is the velocity excursion above average wind speed that is important to capture. Future apparatus design and fan control may enable execution of pre-post lulls in prospective experiments.

In the scaled EVS the uniform velocity field transitions to a highly sheared flow (~7 m/s velocity shear over 2.2 m distance) and then back to a uniform field, again in 5 seconds (Figure 2-8d).

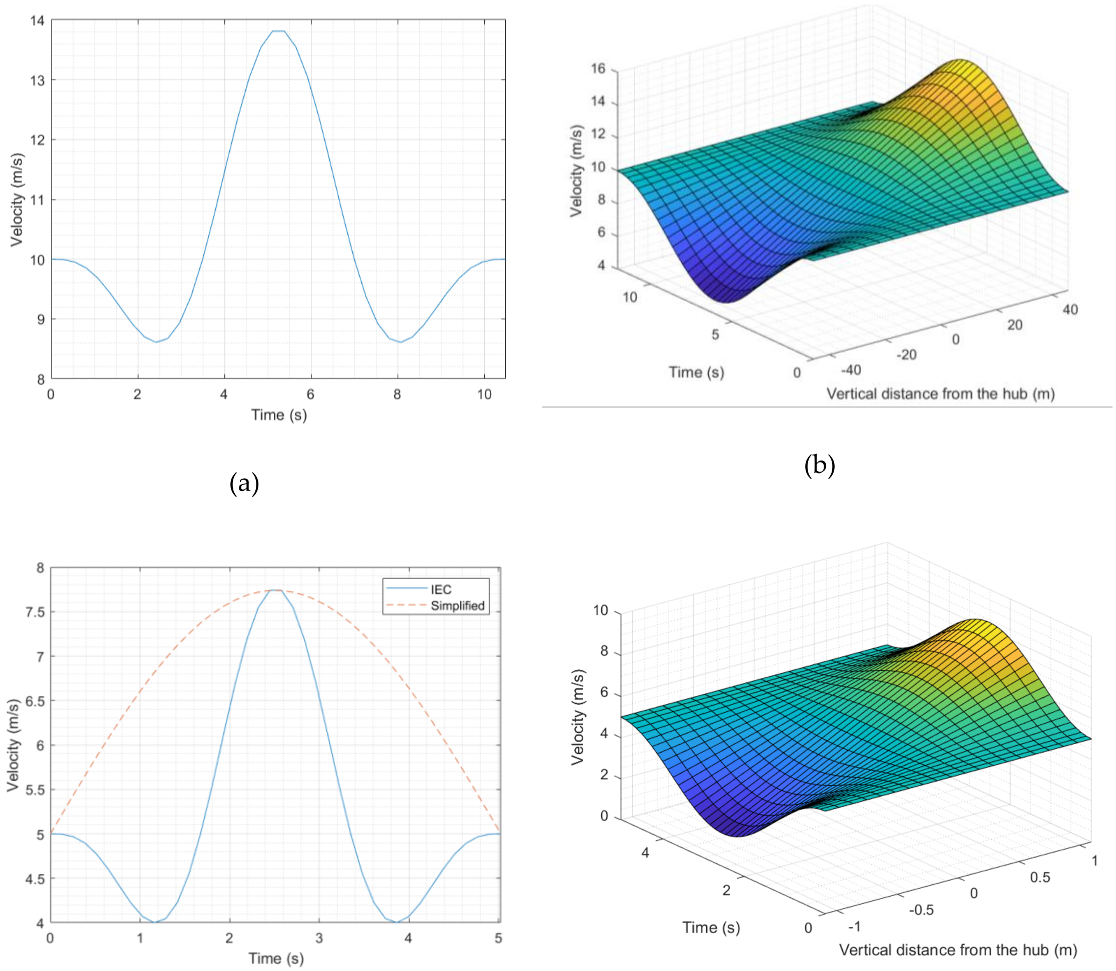

(a) (b)

(c) (d)

Figure 2-8. The extreme operational conditions for a full scale HAWT class B-III with 92 m diameter and hub height of 80m at 10 m/s uniform wind speed compared with the scaled conditions for a B-III turbine with 2.2 m diameter and 2 m hub height at 5 m/s average wind speed (a) full scale extreme operational gust, (b) full scale extreme vertical shear, (c) scaled extreme operating gust, the solid blue line is for IEC and the simplified gust that actually was targeted is in red dashed-line, (d) scaled extreme vertical shear

In these settings, the length and time scale ratios are 5.2 and 2.4 respectively. The Reynolds number based on the relative velocity and chord size at the 70% blade span for full scale turbine at the nominal wind speed and TSR (10 m/s and 8 respectively) is $\sim 7.5 \times 10^6$ and for the scaled turbine at our lab condition is $\sim 32.5 \times 10^3$ which gives the ratio of ~ 230.

2.3 Results and discussion

2.3.1 Steady wind shear

In this section, the simulation cases are all steady and just carried out for the peak stages which is the instantaneous point in time where that maximum shear occurs, as a preliminary investigation to unsteady experiment runs that are examined in the next sub-section. Using the tuned numerical model, the V-c and H-c domains were used to simulate the desired vertical and horizontal sheared flows by modulating the input velocity for the different rows and columns of the fans. The target was to match the velocity profile as similar as possible to the IEC standard for the scaled HAWT, corresponding to ~7 m/s shear while keeping the velocity at the rotor centerline 5 m/s. Figure 2-9 shows the fan setups using CFD for creating the desired shears which could be achieved by using only the 5 fan columns at the middle. For creating negative vertical shear, the setup presented in Figure 2-9a was inverted.

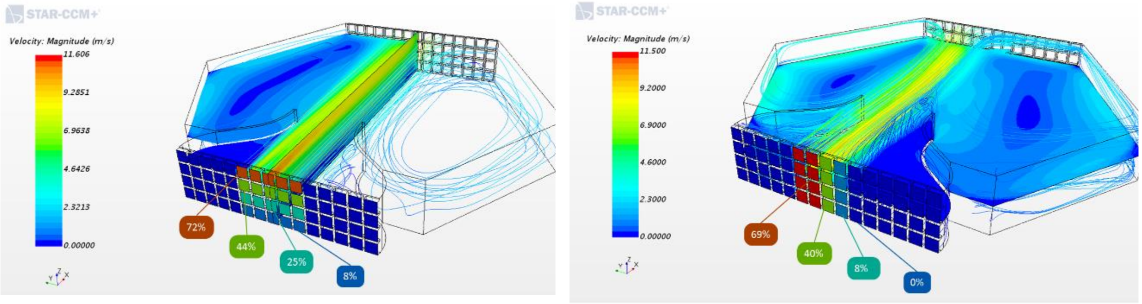

(a) (b)

Figure 2-9. Fan setups for peak stages of extreme (a) vertical and (b) horizontal shears, prescribed for the scaled HAWT identical to full scale condition, the power set-points for each row and columns is included (just the 5 columns at the middle are working)

Using the fan setups shown in Figure 2-9 the physical experiments were carried out and velocity measurements made using the cobra probes. Figure 2-10a, b & c show the average velocity at each probe including the range of velocity fluctuations (standard deviation) compared with average velocity profile from the CFD (dashed-line) and the prescribed shear by IEC standard (yellow solid-line) for the EVS, EHS and negative EVS respectively. The high velocity fluctuations relative to the mean velocity in experiments are due to the strong vortexes that form in these highly sheared flows which increase the momentum mixing at different heights. The amount of shear that was prescribed (∼7 m/s velocity difference) is being successfully created in the tunnel for the positive vertical shear case (Figure 2-10a). However, for the horizontal and negative vertical cases (Figure 2-10b & c) there are larger shears than desired, resulting in a ∼10 m/s velocity difference. From Figure 2-10a & c it is clear that the lower fans work more efficiently than the upper fans (i.e. with the same value of the power set-points, the lower fans generate higher velocities). The largest disconformity exists in the horizontal shear case (Figure 2-10b).

The relative discrepancy between the mean velocity fields of these three experimental steady shears and the IEC are presented in Figure 2-10d. Accordingly, the average amount of disconformities over all of the probes are 41, 27 and 9 % for the horizontal, the negative vertical and the vertical steady shears respectively. Basically, this comparison revealed the capability of the developed numerical model to predict the fan setups for simulating the EWS. As was explained in section 2.2.2, the numerical model is tuned just based on previously tested ABL flows while assuming similar efficiencies for all the fans, neglecting the flow recirculation in the outer shell and simplifying WindEEE test chamber geometry. The fan power values in all the test cases (steady and unsteady) are directly taken from the steady numerical model prediction results. In future, further field adjustments are required to generate a flow field as similar as possible to the IEC prescription.

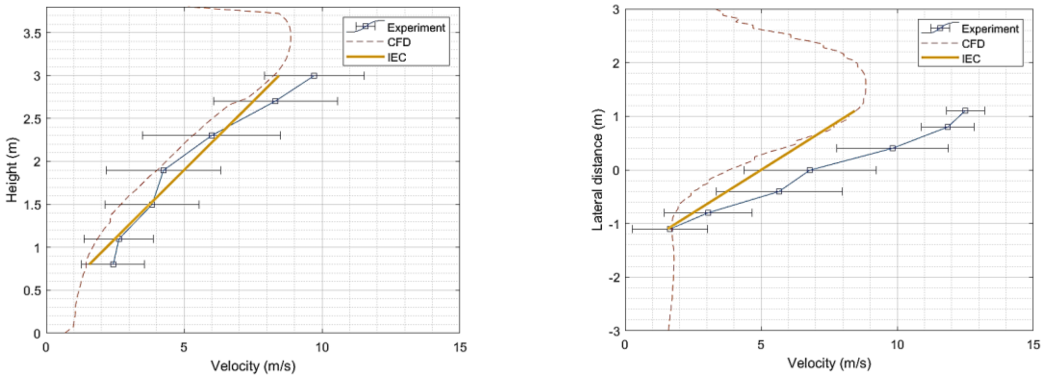

(a) (b)

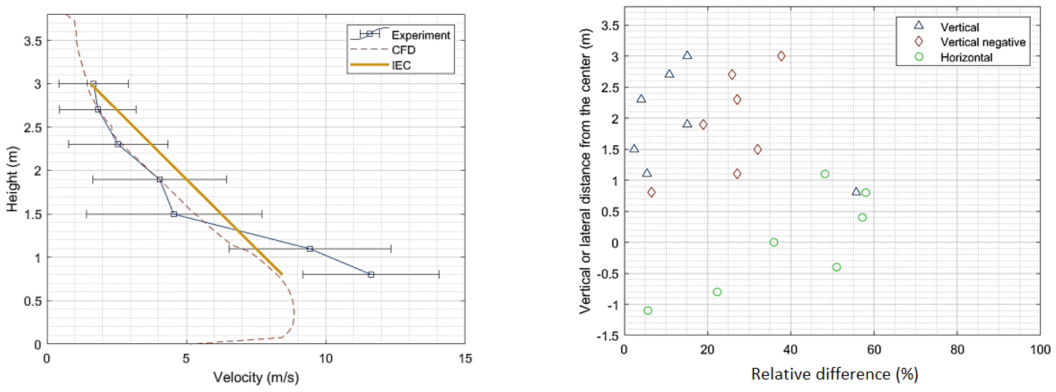

(c) (d)

Figure 2-10: CFD predictions vs experiment data for steady (a) vertical shear, (b) horizontal shear and (c) negative vertical shear, (d) the relative disconformity between experiment and IEC standard

2.3.2 Unsteady experiments

For the shear cases just the five columns of the fans in the middle were working (only 20 out of 60 fans were operated). The uniform flow field before and after the shear events, generated by setting these 20 fans to 39% power. The best results in terms of the event duration, were captured when the extreme condition setups were set for 1.6 s in the actuator software (i.e. the fan powers uniformly stayed at 39% and then switched to the setup in Figure 2-9 for just 1.6 seconds then back to the 39% uniform). The uniform gusts were generated in two ways. The first was again by changing the power set-points of all the 60 fans together. According to the results from the CFD simulations (Domain V-c), in order to achieve the prescribed EOG, the fan power set-points should switch from 17% to 30% and back to the 17% power in the software. For the uniform gust, the best result again was obtained with setting fans to 30% for 1.6 s which resulted in $\sim 5\ s$ uniform gust with desired peak factor. The second way of generating a uniform gust was using the IGVs while keeping fan power set-points constant at 30%. In this run, the actuation frequency of the IGVs was set at 0.05 Hz with a duty cycle of 8%, initial position of 10% open with cycling to 100% open (see section 2.2.1 for IGV setting definitions). In addition, in each uniform gust case, to obtain a better understanding of the uniformity of the flow field, two measurement runs were conducted using both vertical and horizontal layouts of the cobra probes (layouts in Figure 2-6). For processing the data all of the velocity time histories were filtered using a moving average with an averaging window of 0.2 s based on the criteria described at [10].

3D pictures of the filtered turbulent wind fields for the EVS, EHS, negative EVS, EOG cases generated with changing fan powers (vertical & horizontal measurements), and the EOG generated using the IGVs (vertical & horizontal measurements) are presented in Figure 2-11a, b, c, d & e, f & g respectively. The average magnitude of fluctuation around the mean velocity values due to the filtration are ±0.16 m/s for the EWS cases, ±0.11 m/s for the EOG using the fan powers and ±0.41 m/s for the EOG using the IGVs. In Figure 2-11a & c when the 20 fans at middle are operating, it is again evident that the fans at the top row do not work as efficient as the other fans; they could have less stable air supply than the lower rows which should be due to the tight direction change of the recirculating flow from the top. Figure 2-11d & f show velocity fields when all 60 the fans are operating with the contraction walls to help unifying the flow field. Figure 2-11b, e & g show that all of the flow fields are horizontally uniform. The data from the EOG generation with IGVs (which work in a cyclic manner) in Figure 2-11f & g shows the background velocity fluctuations are high relative to the EOG generation by manipulating the fans' powers in Figure 2-11d & e.

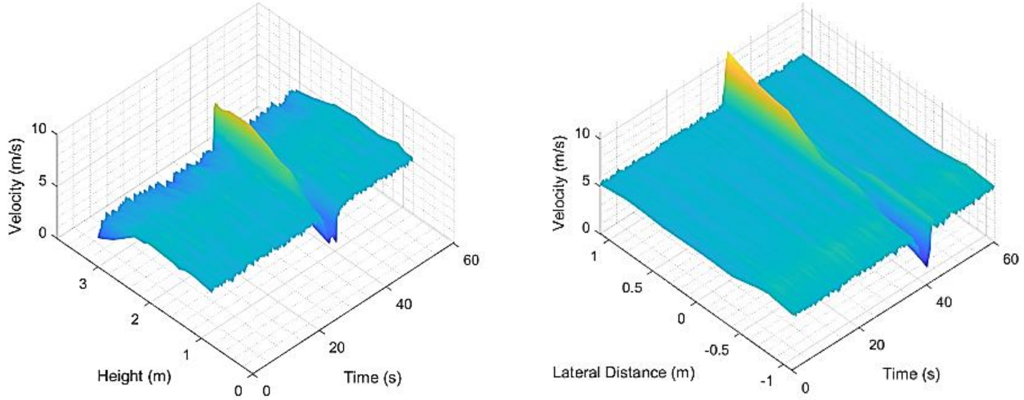

(a) EVS

(b) EHS

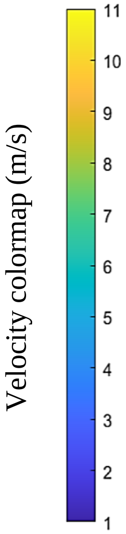

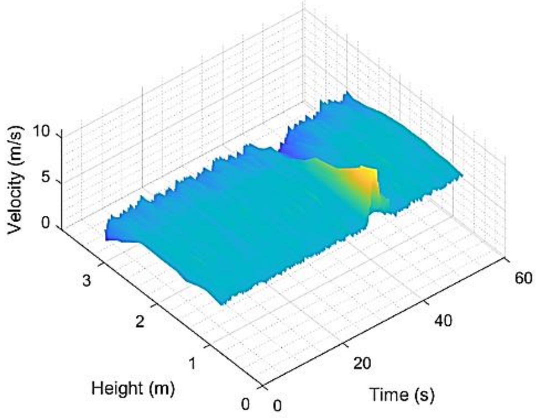

(c) negative EVS

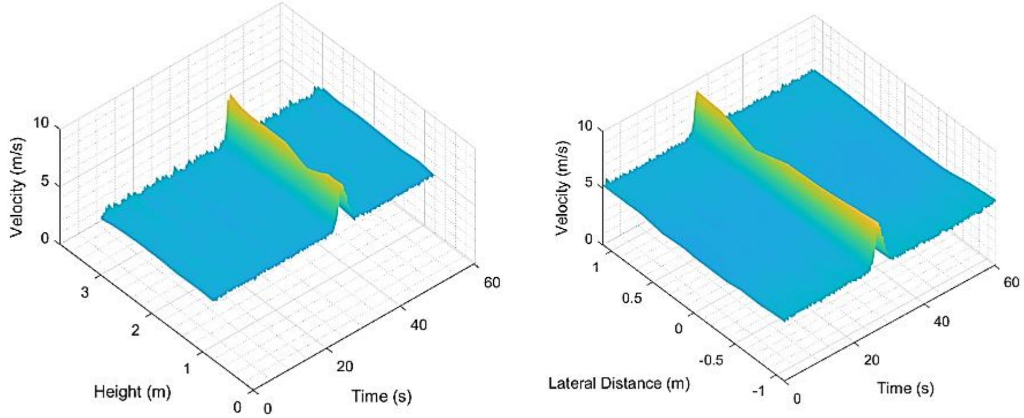

(d) EOG generated with changing fan powers, vertical measurements

(e) EOG generated with changing fan powers, horizontal measurements

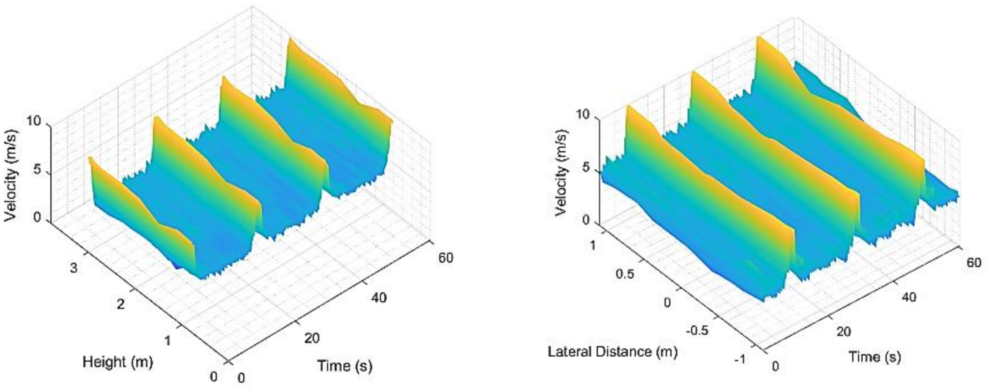

(f) EOG generated with IGVs, vertical measurements

(g) EOG generated with IGVs, horizontal measurements

Figure 2-11. 3D pictures of the complete time history of the phased averaged (with 0.2 s averaging window) turbulent velocity field

In order to have a better comparison of these unsteady cases with the IEC, the velocity time history extracted from the cobra probes B to H (with the layout showed in Figure 2-6) in blue solid-lines along with the standard specifications in orange solid-lines are plotted in Figure 2-12 at the left columns (cases are in the same order as Figure 2-11). The right columns contain the relative instantaneous discrepancy of the velocity relative to the IEC prescribed velocity, normalized by the average velocity ($\sim 5\ m/s$).

Based on data for the shear cases, at the peak stages the amount of desired shear is successfully being generated. However, due to the difference in velocities, there is a time lag between the peaks' locations at the top to bottom heights of the EVS cases, and left to right in the EHS cases (Figure 2-12a, b and c).

As previously discussed, when just the 20 fans in the middle are working the lower efficiency of the top row of the fans is more noticeable at probe H in Figure 2-12a & c; the velocity time history at this height and condition has more fluctuations compared to the other probes. Probe H in Figure 2-12d & f shows in better detail that using all the 60 fans and the contraction walls helps homogenizing the flow field close to the ceiling (i.e. similar velocity magnitudes and fluctuations in all the time histories across the probes). Yet, in the gust peak when the flow is highly dynamic, the insufficiency of the air supply for the top row is noticeable as the probe H in Figure 2-12d demonstrates (the sudden velocity drop while the velocity in other probes are consistently increasing). Similar velocity instabilities have been observed at the same height in other experiment runs when rapid fan power changes were applied. Figure 2-12d & e in detail present the flow field of the EOG generated by changing the whole 60 fans' powers. As the discrepancy time histories suggests, the generated EOGs with this method are consistent with the target simplified gust. However, the profiles are slightly asymmetric; the left side of the gust profiles have positive curvature and the right sides have linear behaviors. This could be due to the fact that the fans do not decelerate as fast as they can accelerate (the gust falling time is not as fast as its rising time). Active fan braking might be explored in future work to accelerate the falling gusts, instead of relying on inertia/friction.

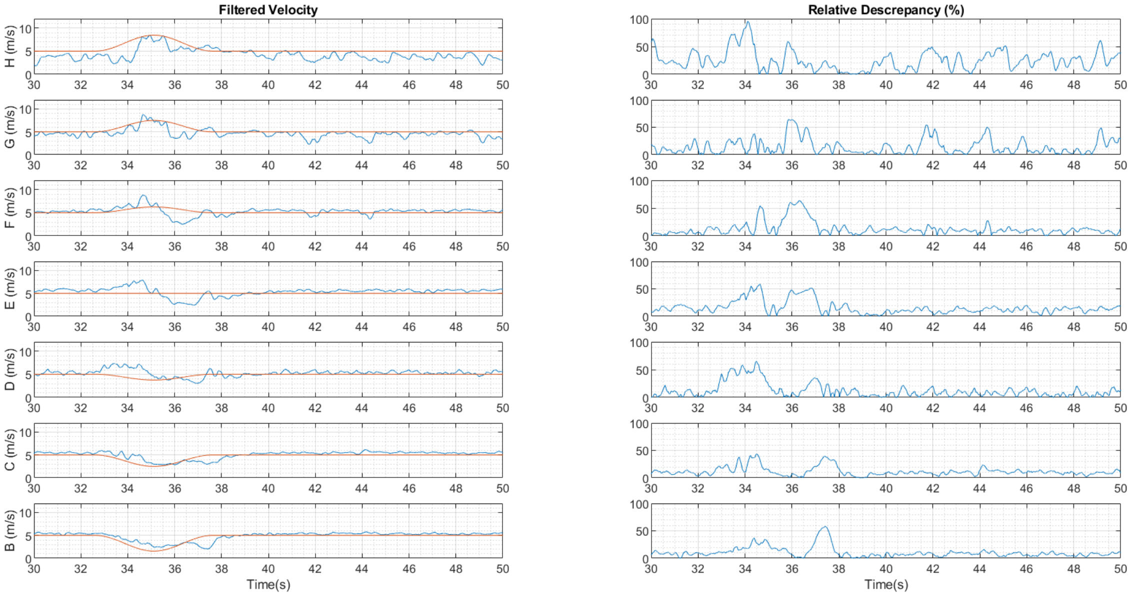

(a) EVS

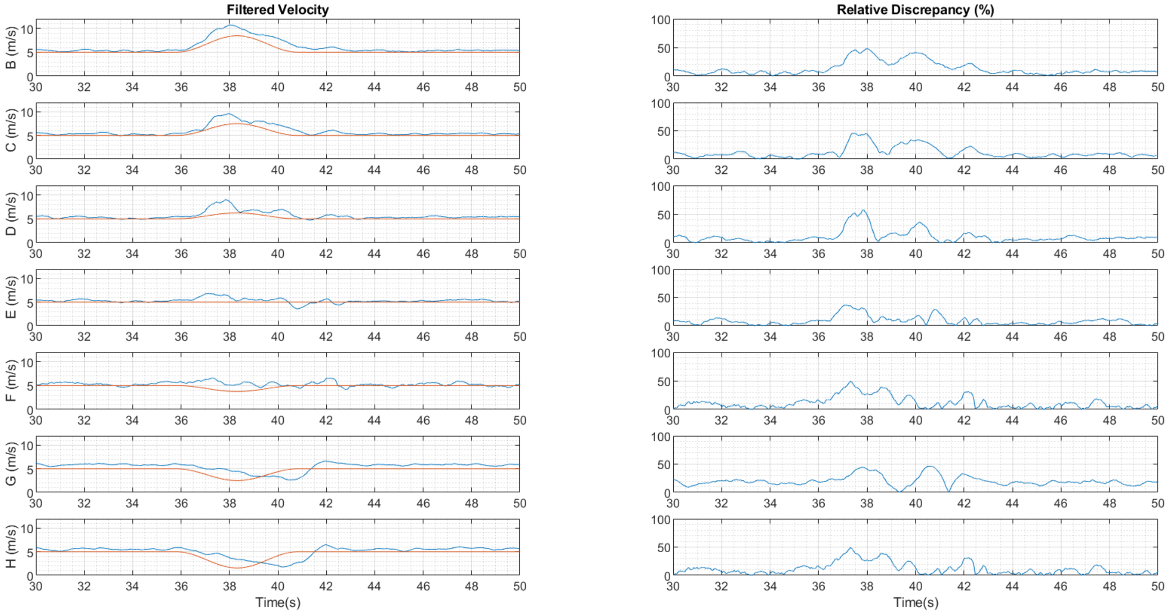

(b) EHS

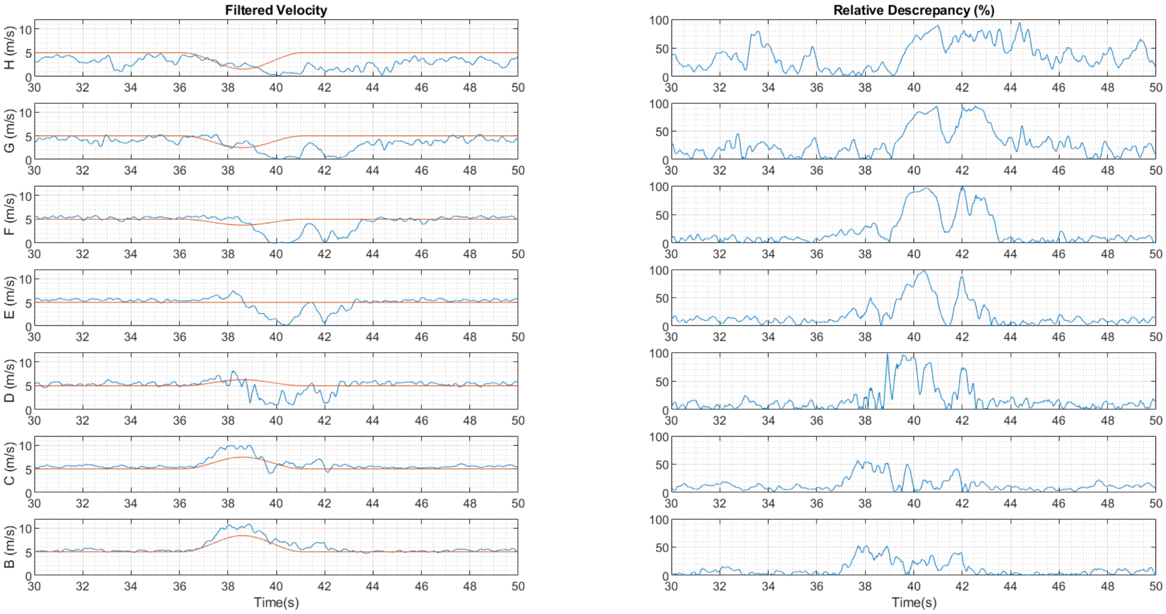

(c) negative EVS

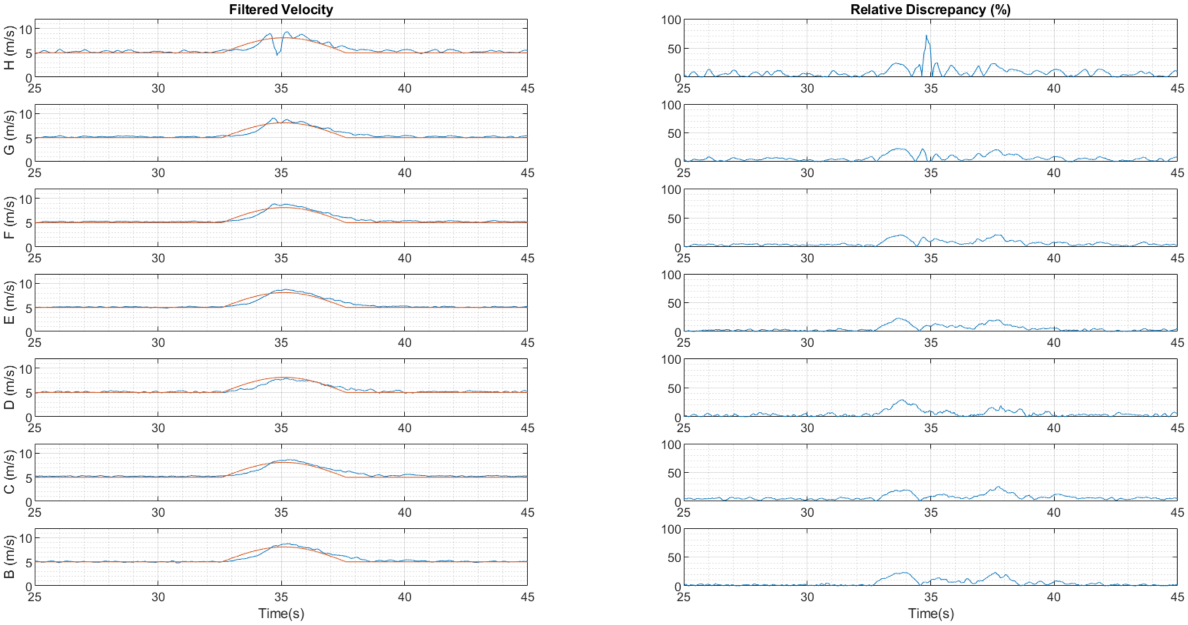

(d) EOG generated with changing fan powers, vertical measurements

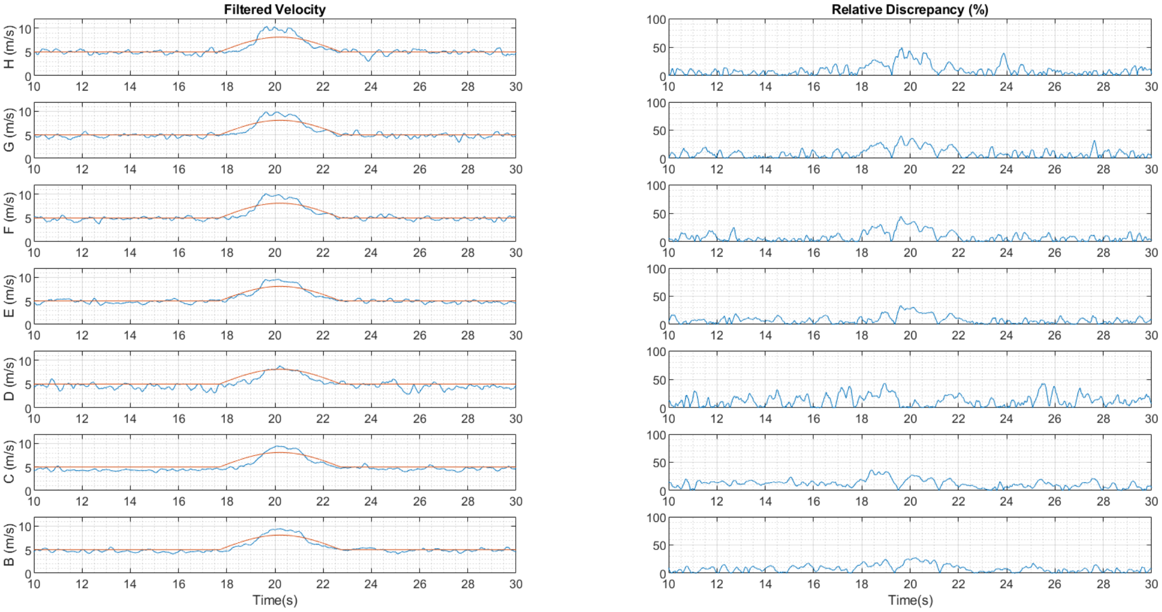

(e) EOG generated with changing fan powers, horizontal measurements

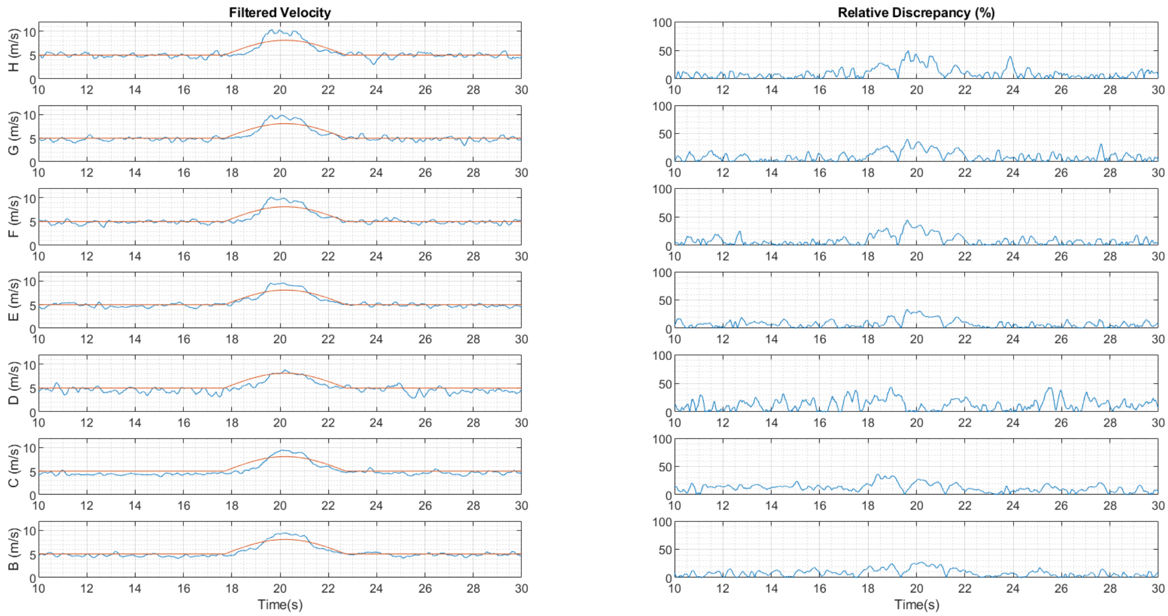

(f) EOG generated with IGVs, vertical measurements

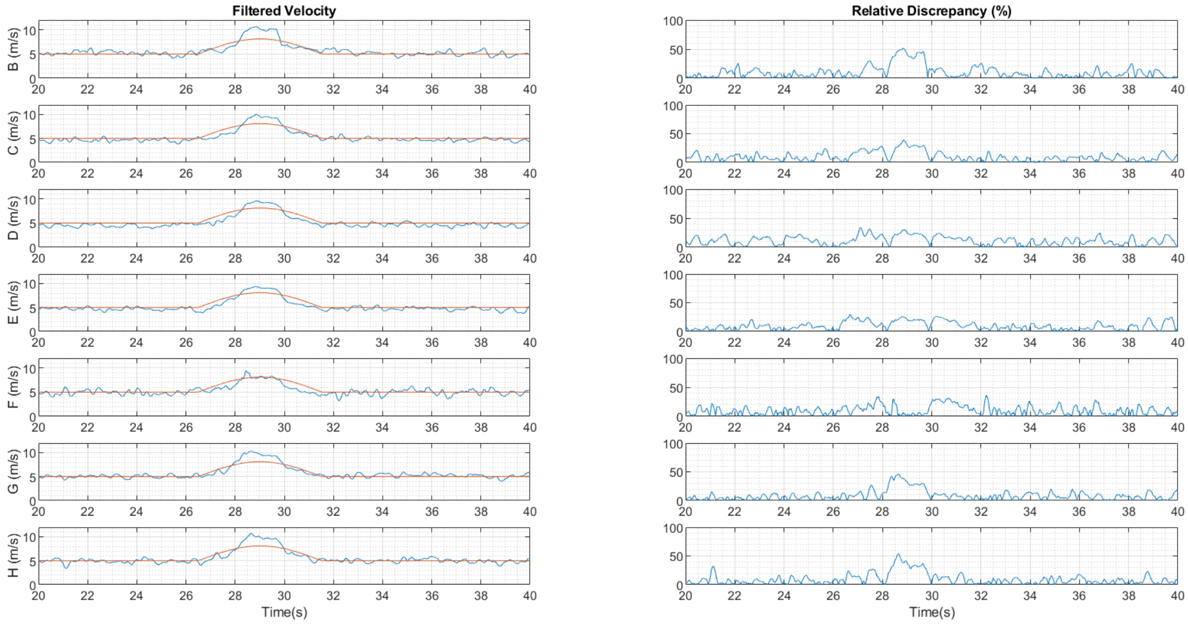

(g) EOG generated with IGVs, horizontal measurements

Figure 2-12. Filtred velocity time history at each probe (with the layout presented in Figure 2-7) as solid blue line compared with prescribed extreme velocity as a solid orange line (left column), time history of relative instantaneous velocity discrepancy normalized by average velocity (right column)

The most consistent EOG was generated by using IGVs in terms of uniformity, symmetry and peak factor at the test section (Figure 2-12f & g). The only noticeable inconsistency of this simulated EOG is due to effect of the contractions walls resulted in slightly higher velocity peaks in probe H and B in Figure 2-12g that are in 1.1 m offset from the center. The generated gust also has positive curvature on the both rising and falling sides. Even though, the simplified target gust has a negative curvature.

2.4 Conclusion

A hybrid experimental/numerical study has been carried out to investigate the possibility of creating extreme conditions for a scaled HAWT based on the IEC 61400-1 standard, in particular the EOG and EWSs, using a unique 60 fan setup in the WindEEE dome at Western University. These conditions were tailored for a 2.2 m diameter test HAWT with the aim to further relate this work to full-scale wind turbines. Therefore, a length and time scaling approach based on tip vortex propagation in the wake was introduced. The resulting time scale is a function of the free stream velocity, tip speed ratio and diameter of the rotor.

A simplified numerical model was first developed and tuned based on a set of steady ABL flow data; the model used a simplified geometry of the WindEEE testing chamber and did not simulate the flow recirculation in the outer shell. The model also treated the fans simply as velocity inlet boundary conditions with the same efficiencies. Yet, it gave a good understanding of the relation between fan power set-points and the flow field at relevant part of the test chamber, which then was used to predict the fan setups for the physical simulation of the extreme events. For future target scenarios the numerical model can be useful to obtain the primary setup, however field adjustments are recommended.

Steady experiment runs corresponding to the peak of the shear cases showed that the fans act non-linearly having different individual efficiencies, especially the top and bottom rows due to the sharp recirculation angle at the suction side of the 60 fan wall. This has not been taken into account in the simplified CFD model and consequently resulted in discrepancies between experiments and the standard shear. By quantifying these discrepancies, corrections can be applied to improve the replication of these events. The unsteady shear flow experiments showed that even though the desired peak factor was generated the high and low velocity peaks reach the test section with a time lag. This can be corrected in the future by providing a phase difference in actuations between the top and bottom rows of fans.

In generation of the EOG by dynamic change of the fan powers, the flow field was more consistent than the EWS compared to their own baselines; the combination of 60 operating fans and the contraction walls helped unifying the flow field. Yet, in fast power transitions due to the sharp recirculation angle the flow field showed some unpredictability and inconsistency close to the ceiling of the test chamber. Generating uniform gusts using the IGVs produced the best results in terms of time scale and peak factor, as well as flow field uniformity and reproducibility. Considering the simplified gust profile without the velocity drops, the generated gust imitates the simplified theoretical profile.

Overall, this study demonstrated promising results using a hybrid numerical/experimental approach for the simulation of extreme wind conditions. These extreme gust conditions can be used with minor modifications in future physical tests to investigate their effects on different aspects of wind turbines' performances. Furthermore, a detail investigation into the reproducibility of these extreme events, specifically the cases generated by dynamic change of the fan powers, is recommended.

2.5 References

[1] F. Ueckerdt, L. Hirth, G. Luderer, and O. Edenhofer, "System LCOE: What are the costs of variable renewables?," *Energy*, vol. 63, pp. 61–75, Dec. 2013, doi: 10.1016/j.energy.2013.10.072.

[2] IEC, "(International Electrotechnical Commission) IEC 61400-1: Wind turbines - Part 1: Design requirements, 3rd ed.," Geneva, Switzerland, 2005.

[3] P. W. Cheng and W. A. A. . Bierbooms, "Distribution of extreme gust loads of wind turbines," *Journal of Wind Engineering and Industrial Aerodynamics*, vol. 89, no. 3, pp. 309–324, 2001, doi: https://doi.org/10.1016/S0167-6105(00)00084-2.

[4] K. S. Hansen and G. C. Larsen, “Full scale experimental analysis of extreme coherent gust with wind direction changes (EOD),” *Journal of Physics: Conference Series*, vol. 75, p. 012055, Jul. 2007, doi: 10.1088/1742-6596/75/1/012055.

[5] M. Wächter, H. Heibelmann, M. Holling, A. Morales, P. Milan, T. Mucke, J. Peinke, N. Reinke, and P. Rinn,“The turbulent nature of the atmospheric boundary layer and its impact on the wind energy conversion process,” *Journal of Turbulence*, vol. 13, pp. 1–21, 2012, doi: 10.1080/14685248.2012.696118.

[6] W. Hu, F. Letson, R. J. Barthelmie, and S. C. Pryor, “Wind gust characterization at wind turbine relevant heights in moderately complex terrain,” *Journal of Applied Meteorology and Climatology*, vol. 57, no. 7, pp. 1459–1476, Jul. 2018, doi: 10.1175/JAMC-D-18-0040.1.

[7] IEC, “(International Electrotechnical Commission) IEC 61400-1: Wind energy generation systems - Part 1: Design requirements, 4th ed.,” Geneva, Switzerland, 2019.

[8] T. Burton, N. Jenkins, D. Sharpe, and E. Bossanyi, *Wind Energy Handbook*, 2nd ed. Chichester, UK: John Wiley and Sons Ltd, 2011.

[9] I. Suomi, T. Vihma, S.-E. Gryning, and C. Fortelius, “Wind-gust parametrizations at heights relevant for wind energy: a study based on mast observations,” *Quarterly Journal of the Royal Meteorological Society*, vol. 139, no. 674, pp. 1298–1310, Jul. 2013, doi: 10.1002/qj.2039.

[10] J. Chowdhury, J. Chowdhury, D. Parvu, M. Karami, and H. Hangan, “Wind flow characteristics of a model downburst,” in *American Society of Mechanical Engineers, Fluids Engineering Division (Publication) FEDSM*, 2018, vol. 1, doi: 10.1115/FEDSM2018-83443.

[11] A. I. Estanqueiro, “A dynamic wind generation model for power systems studies,” *IEEE Transactions on Power Systems*, vol. 22, no. 3, pp. 920–928, Aug. 2007, doi:

10.1109/TPWRS.2007.901654.

[12] M. Anvari, G. Lohman, M. Wachter, P. Milan, E. Lorenz, D. Heinemann, M.R. Rahimi Tabar, and J. Peinke, “Short term fluctuations of wind and solar power systems,” *New Journal of Physics*, vol. 18, no. 6, p. 063027, Jun. 2016, doi: 10.1088/1367-2630/18/6/063027.

[13] M. O. Hansen, *Aerodynamics of wind turbines*, Third ed. Abingdon, UK: Routledge, 2015.

[14] A. Pace, K. Johnson, and A. Wright, “Preventing wind turbine overspeed in highly turbulent wind events using disturbance accommodating control and light detection and ranging,” *Wind Energy*, vol. 18, no. 2, pp. 351–368, Feb. 2015, doi: 10.1002/we.1705.

[15] M. A. Lackner and G. A. M. Van Kuik, “The performance of wind turbine smart rotor control approaches during extreme loads,” *Journal of Solar Energy Engineering, Transactions of the ASME*, vol. 132, no. 1, pp. 0110081–0110088, Feb. 2010, doi: 10.1115/1.4000352.

[16] D. Schlipf, D. J. Schlipf, and M. Kühn, “Nonlinear model predictive control of wind turbines using LIDAR,” *Wind Energy*, vol. 16, no. 7, pp. 1107–1129, Oct. 2013, doi: 10.1002/we.1533.

[17] E. A. Bossanyi, A. Kumar, and O. Hugues-Salas, “Wind turbine control applications of turbine-mounted LIDAR,” *Journal of Physics: Conference Series*, vol. 555, p. 012011, Dec. 2014, doi: 10.1088/1742-6596/555/1/012011.

[18] D. Micallef and T. Sant, “Rotor aerodynamics in sheared inflow: An analysis of out-of-plane bending moments,” *Journal of Physics: Conference Series*, vol. 1037, p. 022027, Jun. 2018, doi: 10.1088/1742-6596/1037/2/022027.

[19] N. Sezer-Uzol and O. Uzol, “Effect of steady and transient wind shear on the wake structure and performance of a horizontal axis wind turbine rotor,” *Wind Energy*,

vol. 16, no. 1, pp. 1–17, Jan. 2013, doi: 10.1002/we.514.

[20] M. Hansen, *Aerodynamics of wind turbines*. 2015.

[21] K. Gharali and D. A. Johnson, “Effects of nonuniform incident velocity on a dynamic wind turbine airfoil,” *Wind Energy*, vol. 18, no. 2, pp. 237–251, Feb. 2015, doi: 10.1002/we.1694.

[22] X. Shen, X. Zhu, and Z. Du, “Wind turbine aerodynamics and loads control in wind shear flow,” *Energy*, vol. 36, no. 3, pp. 1424–1434, Mar. 2011, doi: 10.1016/j.energy.2011.01.028.

[23] M. S. Jeong, S. W. Kim, I. Lee, and S. J. Yoo, “Wake impacts on aerodynamic and aeroelastic behaviors of a horizontal axis wind turbine blade for sheared and turbulent flow conditions,” *Journal of Fluids and Structures*, vol. 50, pp. 66–78, Oct. 2014, doi: 10.1016/j.jfluidstructs.2014.06.016.

[24] K. Thomsen and P. Sørensen, “Fatigue loads for wind turbines operating in wakes,” *Journal of Wind Engineering and Industrial Aerodynamics*, vol. 80, no. 1–2, pp. 121–136, Mar. 1999, doi: 10.1016/S0167-6105(98)00194-9.

[25] F. González-Longatt, P. P. Wall, and V. Terzija, “Wake effect in wind farm performance: Steady-state and dynamic behavior,” *Renewable Energy*, vol. 39, no. 1, pp. 329–338, Mar. 2012, doi: 10.1016/j.renene.2011.08.053.

[26] N. N. Sørensen, J. A. Michelsen, and S. Schreck, “Navier-Stokes predictions of the NREL phase VI rotor in the NASA Ames 80 ft × 120 ft wind tunnel,” *Wind Energy*, vol. 5, no. 2–3, pp. 151–169, Apr. 2002, doi: 10.1002/we.64.

[27] H. Snel, J. G. Schepers, and B. Montgomerie, “The MEXICO project (Model Experiments in Controlled Conditions): The database and first results of data processing and interpretation,” in *Journal of Physics: Conference Series*, 2007, vol. 75, no. 1, doi: 10.1088/1742-6596/75/1/012014.

[28] S. Ricci, A. De Gaspari, L. Riccobene, and F. Fonte, “Design and Wind Tunnel

Test Validation of Gust Load Alleviation Systems,” Jan. 2017, doi: 10.2514/6.2017-1818.

[29] P. M. G. J. Lancelot, J. Sodja, N. P. M. Werter, and R. De Breuker, “Design and testing of a low subsonic wind tunnel gust generator,” *Advances in Aircraft and Spacecraft Science*, vol. 4, no. 2, pp. 125–144, Mar. 2017, doi: 10.12989/aas.2017.4.2.125.

[30] V. Petrović, F. Berger, L. Neuhaus, M. Hölling, and M. Kühn, “Wind tunnel setup for experimental validation of wind turbine control concepts under tailor-made reproducible wind conditions,” in *Journal of Physics: Conference Series*, 2019, vol. 1222, no. 1, doi: 10.1088/1742-6596/1222/1/012013.

[31] T. T. B. Wester, G. Kampers, G. Gulker, J. Peinke, U. Cordes, C. Tropea, and M. Holling, “High speed PIV measurements of an adaptive camber airfoil under highly gusty inflow conditions,” in *Journal of Physics: Conference Series*, 2018, vol. 1037, no. 7, doi: 10.1088/1742-6596/1037/7/072007.

[32] I. Neunaber and C. Braud, “First characterization of a new perturbation system for gust generation: the chopper,” *Wind Energy Science*, vol. 5, no. 2, pp. 759–773, Jun. 2020, doi: 10.5194/wes-5-759-2020.

[33] H. Hangan, M. Refan, C. Jubayer, D. Romanic, D. Parvu, J. LoTufo, and A. Costache, “Novel techniques in wind engineering,” *Journal of Wind Engineering and Industrial Aerodynamics*, vol. 171, pp. 12–33, Dec. 2017, doi: 10.1016/j.jweia.2017.09.010.

[34] H. Hangan, M. Refan, C. Jubayer, D. Parvu, and R. Kilpatrick, “Big data from big experiments. The WindEEE Dome,” in *Whither Turbulence and Big Data in the 21st Century?*, Springer International Publishing, 2016, pp. 215–230.

[35] TFI Ltd., “Cobra Probe,” *Turbulent Flow Instrumentation Pty Ltd*, 2011. https://www.turbulentflow.com.au/Products/CobraProbe/CobraProbe.php (accessed Jun. 12, 2020).

[36] M. Refan and H. Hangan, “Near surface experimental exploration of tornado vortices,” *Journal of Wind Engineering and Industrial Aerodynamics*, vol. 175, 2018, doi: 10.1016/j.jweia.2018.01.042.

[37] D. Romanic, J. LoTufo, and H. Hangan, “Transient behavior in impinging jets in crossflow with application to downburst flows,” *Journal of Wind Engineering and Industrial Aerodynamics*, vol. 184, 2019, doi: 10.1016/j.jweia.2018.11.020.

[38] M. Refan and H. Hangan, “Aerodynamic performance of a small horizontal axis wind turbine,” *Journal of Solar Energy Engineering, Transactions of the ASME*, vol. 134, no. 2, 2012, doi: 10.1115/1.4005751.

Chapter 3

3 Investigation the loads and performance of a model horizontal axis wind turbine under reproducible IEC extreme operational condition©

The power performance and loading dynamic responses of a 2.2 m scaled horizontal axis wind turbine (HAWT) under the IEC 61400-1 transient operational extreme conditions were investigated. Extreme wind shears (EWS) and extreme operational gust (EOG) inflow conditions, generated in the WindEEE dome at Western University. The global forces were measured by a multi axis force balance at the HAWT tower base. The unsteady horizontal shear induced a significant yaw moment on the rotor with similar dynamic loads as the extreme event with no serious effect on the power generation. The EOG severely affected all the performance parameters of the turbine which were highly dependent on the operational TSR and the time duration of the event.

3.1 Introduction

In the past two decades, wind energy has grown to become one of the primary sources of energy being installed worldwide in an effort to reduce greenhouse gas emissions. One of the main factors of this increasing trend is the continued decreasing price of energy generated by wind energy devices. It is still expected for this market to grow by having even lower levelized cost of electricity (LCOE) in the near future [1]. This price reduction can be facilitated by more technological advancements (e.g. building larger rotors) and better understanding of the interaction between different wind conditions and the turbines in order to increase the life cycle of these wind energy systems.

© This chapter has been submitted for publication to journal of Wind Energy Sci. under co-authorship of K. Shirzadeh, H. Hangan, C. Crawford and P. Hashemi.

The dynamic nature of the atmospheric boundary layers (ABL) affects all the dynamic outputs of the wind energy systems; these all bring challenges to further growth of the wind energy share in the energy sector. One of the main challenges for todays' wind energy systems are the power generation fluctuations which cause instability in the grid network [2]. It has been reported that the effect of the extreme events can get transferred to the grid with even amplification in magnitudes (amount of power generation is related to the cube of wind velocity); the power output of the whole wind farm can change by 50% in just 2 minutes [3]. These turbulent features also induce fatigue loads on the blades [4] predominantly for the flap wise loadings [5], which then get transferred to the gearbox [6], bearings and then the whole structure. Implementation of LIDAR technology can make revolutionary contribution to this matter by measuring the upstream flow field and give enough time to the control system to properly adjust itself (e.g. blade pitch angles, generator load & etc) in order to reduce overall power fluctuations and the mechanical load variations [7].

During the past few decades some comprehensive design guidelines have been developed in terms of load analysis. The International Electrotechnical Commission (IEC) included some deterministic design load cases for commercial horizontal axis wind turbines (HAWT) in operating condition in the IEC 61400-1 document [8] followed by statistical analysis introduced in the latest edition [9]. Herein we test the power generation and loads on a scaled HAWT for representative deterministic gust design conditions as per third version of the IEC 61400-1. In the last chapter, the development of the corresponding scaled extreme transient wind fields was carried out. More specifically, the extreme operational gust (EOG) and extreme wind shears (EWS) which includes the extreme vertical and horizontal shears (EVS and EHS), were all experimentally simulated in the WindEEE Dome.

From an aerodynamic perspective the effective angle of attack on the blades and consequently the global lift and drag forces increase during wind gust conditions which result in blade's torque, thrust and root moment amplification. Several experimental studies have been conducted to control the rotor aerodynamics under these transient events. The application of the adaptive camber airfoil in a gusty inflow generated by active grid was investigated by Wester et al., 2018 [10]. These type of airfoils have coupled leading and trailing edge flaps, which can be adjusted to de-camber the profile with increasing lift force. This proved to reduce the integral lift force about 20% at the peak in a gust event. Petrović et al., 2019 [11] developed an algorithm for a PI controller of the pitch angles of a scaled wind turbine in the wind gust conditions generated by an active grid. Using the algorithm, they were able to reduce over speeding of the rotor and the blades' bending moments.

The effect of the wind shears on wind turbine aerodynamics has been studied by several investigators. The effect of various shear flows and turbulence intensities, generated by active grid, on the near wake region of a small scaled turbine was investigated by Li et. al. [12] using PIV measurements. It has been found that the absolute mean velocity deficit in this region remains symmetric and it is insensitive to the inflow non-uniformity. Also, the mean power production does not change with the amount of the shear. However, the power fluctuation has a linear correlation with the amount of background turbulence intensity, in other words, the effect of higher shears translated as a higher inflow turbulence and therefore higher fluctuations in power. Similar results were reported by Sezer-Uzol and Uzol [13] who used a three-dimensional unsteady vortex-panel method to investigate the effect of transient EWS on the performance of a HAWT. They found that due to the EWS, the blades experience asymmetrical surface pressure variations. Consequently, the rotor produces power and thrust with high amplitude of fluctuations which cause significant structural issues and reduce the lifetime of the turbine. From the field data perspective it has been reported that for the same reference wind speed, higher turbulence intensities result in relative higher power efficiencies below the nominal operational condition but the efficiency decreases in transition to rated power [14].

The transient flow fields have been previously generated either numerically or physically by means of active grids. While some of these studies reproduced various transient flows, none had attempted to reproduce and apply the EOG and EWS as per IEC standards and compare the results with stationary and uniform inflow conditions which constitutes the main objectives of the present study. Moreover, the present work employs for the first time a matrix of individually controlled fans to generate customized flow fields and investigate their effect on a model scale wind turbine. The work has been done at the WindEEE Dome at Western University Canada. Alongside with the numerical simulations and field data, this setup can contribute to fast development of the new control prototypes of HAWT to customized transient wind fields.

This is an experimental study for examination of the load and power performance of the turbine under four unsteady extreme condition cases (EVS, EHS, negative EVS and EOG), developed in Chapter 2. To provide an examination of changes relative to a baseline reference, the results in each case have been normalized with values from a uniform inflow.

This chapter is organized as follows. Section 3.2 briefly presents the target deterministic operational extreme conditions. Section 3.3 details the WindEEE chamber and the experiment setups; this section also provides the details about the uniform flow fields used as reference values for comparisons. Section 3.4 presents the results from EWSs and EOG. Section 3.5 provides the conclusions.

3.2 Deterministic extreme operating conditions

Prior to introducing the deterministic gust models, it is informative to know how the standard [8] classifies wind turbines based on a reference wind speed and turbulence intensity (TI). The TI in the standard is given for a specific height, and is defined as the ratio of the mean standard deviation of wind speed fluctuations to the mean wind speed value at that height, both calculated in 10 min intervals. Three classes of reference wind speeds (U_{ref}: I, II and III) and three classes of turbulence intensities (I_{ref}: A, B and C) are defined that gives a combination of 9 external turbine design conditions that have specified values. One further class for special conditions (e.g. off-shore and tropical storms) is considered which should be specified by the designer. Correspondingly, an extreme wind speed model as a function of height (Z) with respect to the hub height (Z_{hub}) with recurrence period of 50 years (U_{e50}) and 1 year (U_{e1}), is defined as follows:

$$U_{e50}(z) = 1.4U_{ref}\left(\frac{Z}{Z_{hub}}\right)^{0.11}$$

$$U_{e1}(z) = 0.8U_{e50}(z) \qquad 3\text{-}1$$

Based on the turbulence class, the streamwise hub height velocity standard deviation (σ_u), is defined by what is called the normal turbulence model as equation 3-4.

$$\sigma_u = I_{ref}(0.75\overline{U_{hub}} + 5.6), \qquad 3\text{-}2$$

$\overline{U_{hub}}$ is the average velocity at hub height.

Based on equations 3-2 and 3-1 the hub height gust magnitude (U_{gust}) is given as:

$$U_{gust} = min\left\{1.35(U_{e1} - U_{hub}); 3.3(\frac{\sigma_u}{1 + 0.1\left(\frac{D}{\Lambda_u}\right)})\right\} \qquad 3\text{-}3$$

Taking t as the time and $t = 0$ as the beginning of the gust, the velocity time evolution of the EOG is defined as:

$$U(t) = \begin{cases} \overline{U_{hub}} - 0.37U_{gust}sin\frac{3\pi t}{T}\left(1 - cos\frac{2\pi t}{T}\right); when \quad 0 \le t \le T, \\ \overline{U_{hub}}; \quad when\ t > T\ or\ t < 0, \end{cases} \qquad 3\text{-}4$$

T is the duration of the EOG, specified as 10.5 seconds, D is the diameter of the rotor and Λ_u is the longitudinal turbulence scale parameter which is a function of the hub height:

$$\Lambda_u = \begin{cases} 0.7Z_{hub} & for\ Z_{hub} \le 60\ m, \\ 42\ m & for\ Z_{hub} > 60\ m, \end{cases} \qquad 3\text{-}5$$

The EWS can be added to or subtracted from the main uniform or ABL inflows. The EVS velocity time evolution at a specific height (Z) can be calculated using equation 3-6.

$$U_{EVS}(Z,t) = \begin{cases} \left(\frac{Z - Z_{hub}}{D}\right)\left(2.5 + 1.28\sigma_u\left(\frac{D}{\Lambda_u}\right)^{0.25}\right)\left(1 - \cos\left(\frac{2\pi t}{T}\right)\right); when \quad 0 \le t \le T, \\ 0 \quad ; when\ t > T\ or\ t < 0, \end{cases} \qquad 3\text{-}6$$

The EWS duration is 12 s. For a commercial III_B class HAWT with 92 m diameter and 80 m tower hub height, at 10 m/s average velocity, the prescribed EOG and EVS are presented in Figure 3-1a & b. The time windows in these figures start and end with the extreme event. The standard gust durations in operation condition are relatively long compared to the response time of scaled wind turbines. Herein, we assume these time durations (10.5 s for EOG and 12 s for EWS) correspond to 4 complete rotor revolutions period in commercial wind turbines which typically have a rotational speed in the range of $\sim 15-20\ RPM$; or in another words, the gust time duration is equal to the propagation of the four complete tip vortex loops from a specific blade in the wake. Accordingly, the time scale becomes a function of TSR (i.e. the ratio of the blade tip linear velocity over the free stream), free stream velocity and diameter of the rotor; the length scale is just a function of TSR and diameter of the rotor.

Assuming a similar III_B class HAWT with hub height of ~2 m with the 2.2 m diameter scaled wind turbine, at 5 m/s average hub-height velocity, the extreme condition profiles look identical to the full-scale ones (the same peak factor but different gust time) as presented in Figure 3-1c & d. These are the inflow fields that are considered in the present experiments.

For a scaled wind turbine, the duration corresponding to four revolutions in similar operating conditions is of the order of one second. The experiments in the earlier study showed that the fastest possible gust obtained in the WindEEE Dome with this peak factor is around 5 seconds (see section 2.2.4). Therefore, based on our assumption the turbine should be working at 1.1 TSR. Also due to hardware limitation in the physical experiments the EOG has been simplified by excluding the velocity drops before and after the main peak as it is shown in Figure 3-1c in red-dashed line.

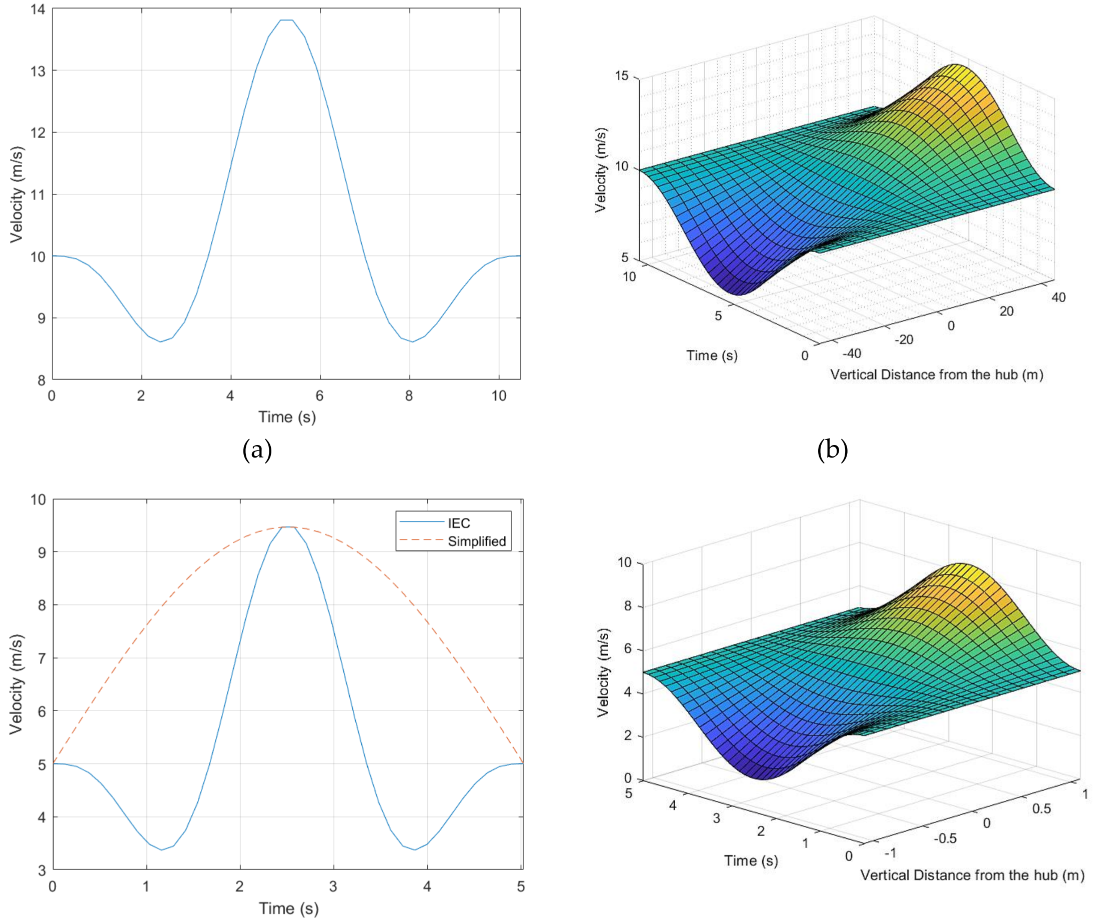

(a) (b)

(c) (d)

Figure 3-1. Extreme operational conditions for a full scale HAWT III_B class with 92m diameter and hub height of 80m at 10 m/s uniform wind speed, (a) extreme operational gust, (b) extreme vertical shear on the rotor with hub height as reference, The scaled extreme condition, (c) the IEC EOG and the simplified EOG that was targeted, (d) extreme vertical shear.

It is worth to mention that these extreme models are relatively simple and not able to capture the real dynamics of the ABL flow-field that directly affect the performance of the turbine [15], [16]. However, it provides practical guidelines for the development and wind tunnel testing of HAWTs.

3.3 Experimental methodology

3.3.1 WindEEE Dome

The experiments were carried out at the Wind Engineering, Energy and Environment (WindEEE) Dome at Western University, Canada. The test chamber has 25 m diameter footprint and 3.8 m height with a total number of 106 fans among which 60 fans mounted along one of the hexagonal walls in a 4×15 matrix and 40 fans are on the rest of the peripheral five walls (Figure 3-2a). 6 other larger fans are in a plenum above the test chamber usually being used for 3D flows like tornado and down bursts [17]. In the present study, experiments were carried out using the dome in 2D flow (e.g. ABL, uniform straight flows and etc.) closed circuit mode which just the 60-fan wall is operated. In this mode the flow recirculates from the top through the outer shell as it is shown in Figure 3-2a. Each of these fans are 0.8 m in diameter and are individually controlled to a percentage of their 30-kW maximum power using variable frequency drives. In order to reach higher velocities at lower fan power set-points at the test chamber for generating EOG a 2D contraction with ratio of 3, was installed just downstream of the 60-fan wall (Figure 3-2a). These fans are equipped with adjustable inlet guiding vanes (IGV). They can be adjusted stationary from 0% open (close) to 100% open or dynamically in a cycle of opening and closing (Figure 3-2b). By using this feature the uniform gusts were produced. The transient shears were produced by power modification of the 5 middle fan columns (20 fans). Therefore, contraction walls had no effect on the EWS flow fields.

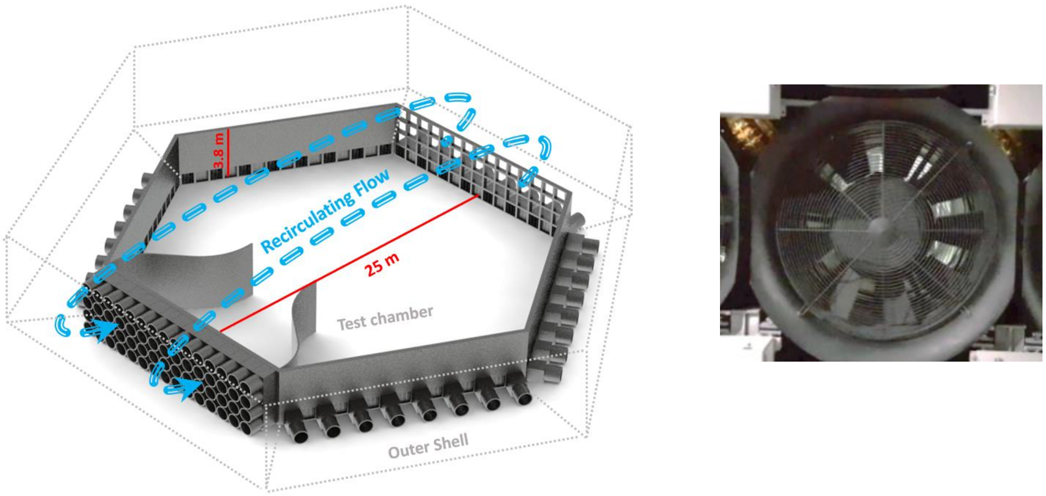

(a) (b)

Figure 3-2. Simplified geometry of the WindEEE dome, (a) the test chamber and the contraction walls with the flow recirculation path through the outer shell in closed circuit 2D flow mode (b) The adjustable vanes at the inlets of the 60 fans at 70% open vanes

3.3.2 The experimental set-up for power and load performance

To measure the velocity of the flow filed, four cobra probes [18] are used in a plane 1 m upstream (~0.5 D) the rotor and 1.3 m offset from the centerline of the primary flow direction. The probes are set at 3 m and 0.8 m heights corresponding to the highest and lowest heights of the rotating blades' tips (Figure 3-3). With this configuration the cobra probes can give a proper perception of the flow field over the wind turbine rotor plane. The wind turbine was mounted on a six-component force balance sensor for measuring all 3 forces/ shears and 3 moments at the base of the tower. After mounting the turbine, the force balance was calibrated as zero in all the axis when turbine was parked and fans were not operating. In addition, a light photoelectric diffuse reflection proximity sensor was used which gives a voltage pulse once it detects a light reflection from the blade passing in front. Using the pulse, one can measure the angular velocity of the rotor with a high resolution (three times a revolution). This wind turbine is equipped with a three phase AC generator. A specific electrical circuit was used to convert the voltage and current to DC and feed the power to the resistors. The last parameter that was monitored was the voltage from the terminals of the power resistors which were set at constant 8.1Ω in order to keep the rotor at the desired TSR (= 1.1). At the end, eight analogue voltage signals (six voltages from force balance, one from proximity sensor and one from load terminals), plus four wind velocity signals gathered to one deck and logged at 2000 Hz frequency for 90 s for each experiment run.

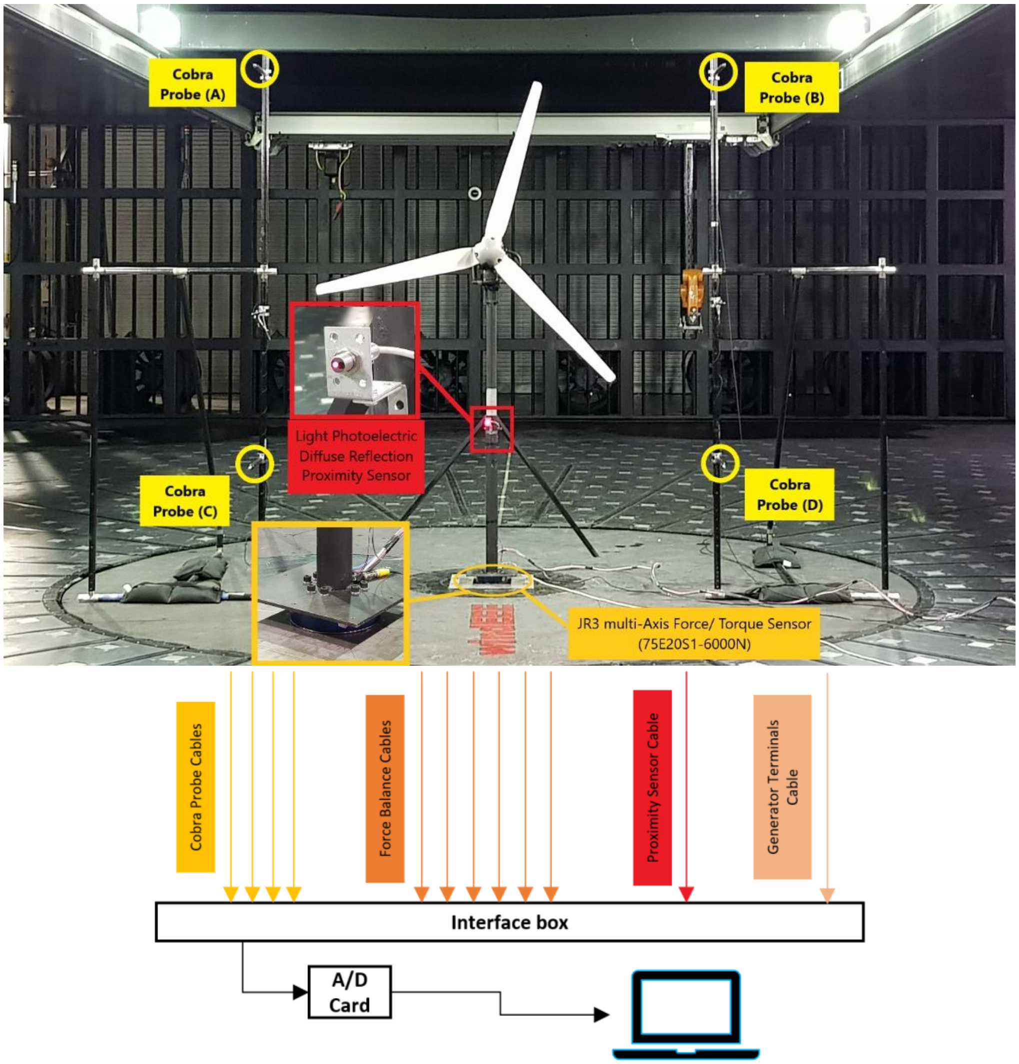

Figure 3-3. Set-up for measuring power generation and dynamic loads for different type of inflow

The schematic of the positioning of the wind turbine and the cobra probes relative to the local coordinate system (centre of the WindEEE dome/ base of the tower) is depicted in Figure 3-4. The shear forces and moments at the base are correlated with the performance of the wind turbine. Based on this local coordinate system, the most important shear force at the base is in the X direction which represents the thrust of the rotor plus the drag force of the tower. The X moment represents torque on the generator plus induced vortex shedding moment; the Y moment shows the bending moment due to drag on the whole structure (correlated to the forces in X direction) and the moment around the Z axis shows the torsion due to horizontal non-uniformity of the flow. The Z force is a measure of how much the turbine gets pushed down or upward during the operation.

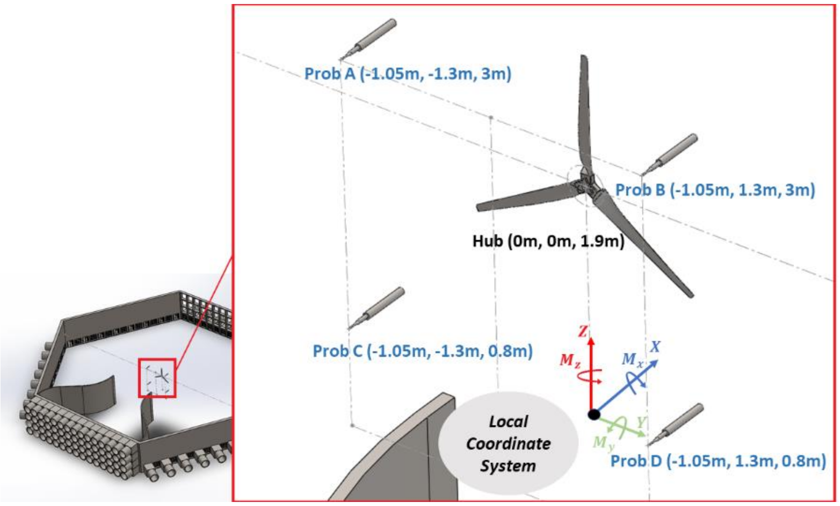

Figure 3-4. The arrangement of cobra probes and HAWT relative to local coordinate system

3.3.3 Baseline uniform inflow experiments

As mentioned earlier, in this study four unsteady extreme condition cases (EVS, EHS, negative EVS and EOG) are considered for the investigation. The results from power performance and loading of each case are normalized with their corresponding averaged data from one of the two different 5 m/s steady uniform wind inflow while the TSR was kept close to 1.1 to match the scaling that was considered. The reason for using different uniform cases is due to the difference in the flow characteristics (TI and spectra) related to the different fan setups for each case. At this low TSR, considerable parts of the blades are in stall and the TI magnitude can affect the flow behavior on the suction side of the blades and result in noticeable difference in loads and power performance of the wind turbine. The mean and RMS values of the data obtained from the force balance, turbine power and TSR from these two uniform cases are tabulated in Table 3-1. The bolded values in this table will be used to normalize the corresponding data from the transient experiment cases.

Table 3-1: The mean values of loads and power generation for different steady uniform cases (with the same load, 8.1$\boldsymbol{\Omega}$)

<table>
<tr><th>5 m/s Uniform Case</th><th>Fan Configuration</th><th>Average wind velocity and TI from all the probes</th><th colspan="4">Turbine Performance
(mean value | standard deviation)</th></tr>
<tr><td rowspan="5">A</td><td rowspan="5"><i>5 columns at middle at 40% and IGVs at 100% open</i>
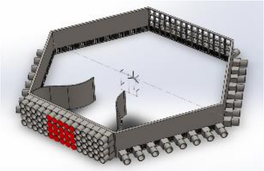</td><td rowspan="5">4.91 m/s,
16%</td><td></td><td><i>x-axis</i></td><td><i>y-axis</i></td><td><i>z-axis</i></td></tr>
<tr><td>Shears (N)</td><td>14.36 | 0.45</td><td>-0.22 | 0.37</td><td>-4.8| 0.69</td></tr>
<tr><td>Moments (Nm)</td><td>0.87 | 0.19</td><td>-20.51 | 0.91</td><td>-0.14 | .25</td></tr>
<tr><td>Electrical power (W)</td><td></td><td>0.81| 0.04</td><td></td></tr>
<tr><td>TSR</td><td></td><td>1.30 | 0.11</td><td></td></tr>
<tr><td rowspan="5">B</td><td rowspan="5"><i>All fans at 30% and IGVs at 10% open</i>
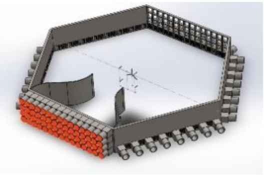</td><td rowspan="5">5.15 m/s,
10%</td><td></td><td><i>x-axis</i></td><td><i>y-axis</i></td><td><i>z-axis</i></td></tr>
<tr><td>Shears (N)</td><td>14.39 | 0.44</td><td>-0.48 | 0.32</td><td>-5.36 | 0.71</td></tr>
<tr><td>Moments (Nm)</td><td>0.84 | 0.16</td><td>-23.06 | 0.92</td><td>-0.25| 0.30</td></tr>
<tr><td>Electrical power (W)</td><td></td><td>0.67 | 0.02</td><td></td></tr>
<tr><td>TSR</td><td></td><td>1.08 | 0.08</td><td></td></tr>
</table>

The turbulence spectra of these two uniform cases are presented in Figure 3-5. There is a consistent noise from the fans with its harmonics at some specific high frequencies. Due to the steadiness of the flow, large share of the energy is distributed at the low-end frequencies (i.e. frequencies lower than 3). In this region, the two cases show the same energy distribution. However, for frequencies higher or equal to 3Hz (based on the frozen turbulence hypothesis corresponds to length scales of 1.65 m and smaller $\{\frac{1}{3}[s] \times 5\left[\frac{m}{s}\right] = 1.65\ [m]\}$), difference in energy distribution is noticeable with lower turbulence energy in case B in all the corresponding frequencies relative to case A. All the spectra follow the -5/3 slope consistent with the Kolmogorov theory in inertial subrange [19].

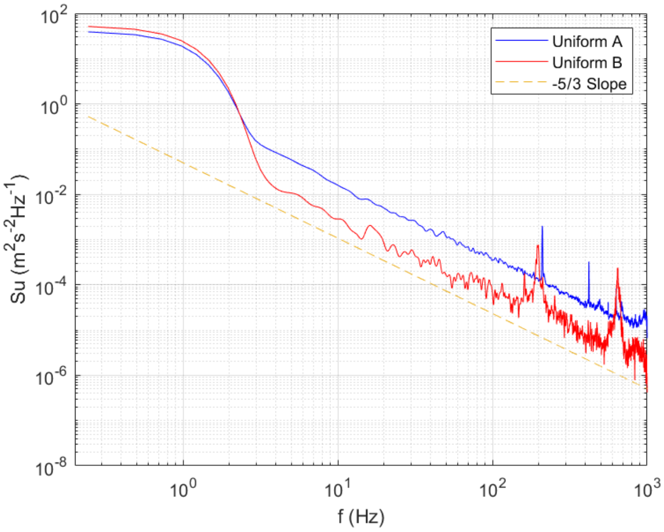

Figure 3-5: Comparison of turbulent velocity spectra for the 5 m/s uniform cases

3.3.4 Uncertainty Analysis

The epistemic uncertainty of the cobra probes depends on turbulence levels but is generally within ±0.5 m/s in average, up to about 30% turbulence intensity according to the manufacturer company [18]. Considering the 5 m/s average wind velocity in the experiments the uncertainty of the probes is 10%. The JR3 multi-axis force/torque sensor (75E20S1-6000N) at the base of the tower has ±0.25% nominal accuracy for all axes. The uncertainly related to measuring and converting the analog voltages to digital for each signal is negligible.

All the values from the measuring instruments presented in section 3.4 have been filtered by moving average method except for rotor speed. The averaging window for wind velocities, generator voltage and load signals were chosen as 0.2, 0.2 and 0.5 second respectively, which preserve the main shape of signal by just filtering low powered high frequency fluctuations. Therefore, the RMS values for aleatoric uncertainty averaged in all the experiments in reading the cobra probes, power are ±0.48 m/s, ±0.04 W; the corresponding values for forces and moments in X, Y and Z axis are ±1.13 N, ±0.69 N, ±0.77 N ±1.52 Nm, ±3.17 Nm, ±0.31 Nm respectively. The combined uncertainties in percentage of their corresponding mean values are tabulated in Table 3-2. The large percentage error in some of the qualities are due to their very small corresponding average values.

Table 3-2. The combined uncertainty estimation of the measured values averaged in all the experiments

	Epistemic uncertainty	Aleatoric uncertainty	Combined uncertainty
Wind velocity	±10%	±9.60%	±13.86%
Power	±0 %	±5.71%	±5.71%
X-force	±0.25%	±7.86%	±7.86%
Y-force	±0.25%	±114.12%	±114.12%
Z-force	±0.25%	±15.42%	±15.42%
X-moment	±0.25%	±178.21%	±178.21%
Y-moment	±0.25%	±13.78%	±13.78%
Z-moment	±0.25%	±125.54%	±125.54%

3.4 Turbine test case results

3.4.1 Unsteady EWS

The time history of the results from EVS, negative EVS and EHS cases generated by changing the fan power set-points are presented in Figure 3-6a , b and c respectively. There are five windows in all of these sub-figures; the first window at the top shows the filtered wind velocity time histories from the four probes; next window shows the electrical power performance along with TSR; next three windows show the filtered forces and moments time histories exerted at the tower base. The stared axis indexes are normalized by their corresponding values from uniform case A. The second window in all the Figure 3-6a, b & c illustrates these transient shear cases do not have a significant effect on the overall power performance of the wind turbine. The initial increase and decrease in power productions are just due to the time lag ($\sim 1.5\ s$) between the high and the low peaks of the shears hitting the rotor which is more noticeable from cobra probes time history in Figure 3-6c.

The EVSs (Figure 3-6a & b) do not have any significant effect on the loads at the base of the tower either. The slight observed rise and fall in the loads at the tower base is due to the time lag that was mentioned above. These extreme shears could induce severe fatigue loads at the blade’s bearing, blade’s root, and the yaw bearing. Having load cells at the blades’ roots and nacelle-tower junction or yaw bearing could have given more information about the loads’ dynamics and the out-of-plane moment in these scenarios.

The correlation between force in X axis and moment around Y axis is clearly visible in all these figures. The Y force shows completely random dynamics with no correlation with the forces and moments in other directions. The Z force maintained the same values in these EWSs but shows no correlation with other loads. The X moment which represents both the vortex shedding and the torque on the generator has the strongest fluctuation compare to the Y and Z moments time histories. The Z moment in the two EVS cases is a small fluctuating value close to zero due to slight horizontal non-homogeneity of the flow-field. Theoretically, it should remain the same even at the time EVSs happen but as Figure 3-6a & b demonstrate there are small variation in the Z moments which can be due to different efficiency of the fans in acceleration and deceleration.

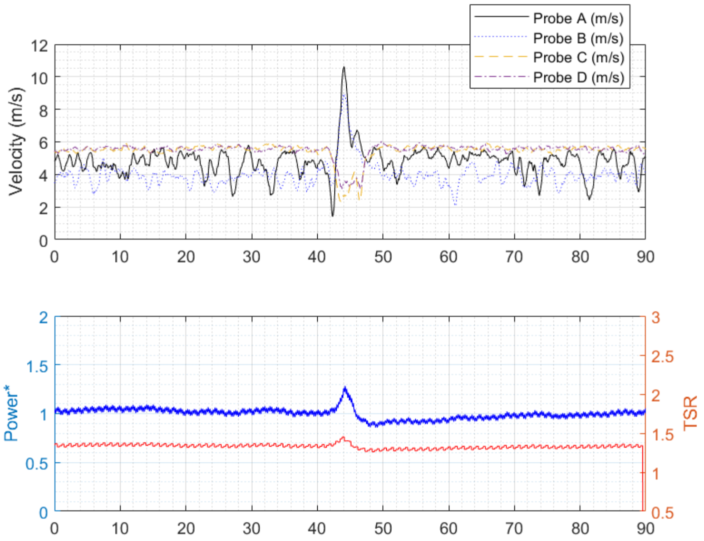

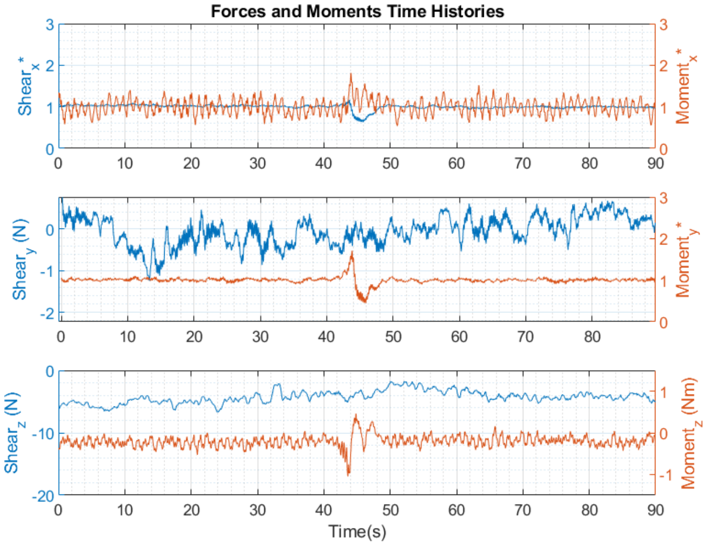
Forces and Moments Time Histories
Shear*x
Moment*x
Shear_y (N)
Moment*y
Shear_z (N)
Moment_z (Nm)
Time(s)

(a) EVS

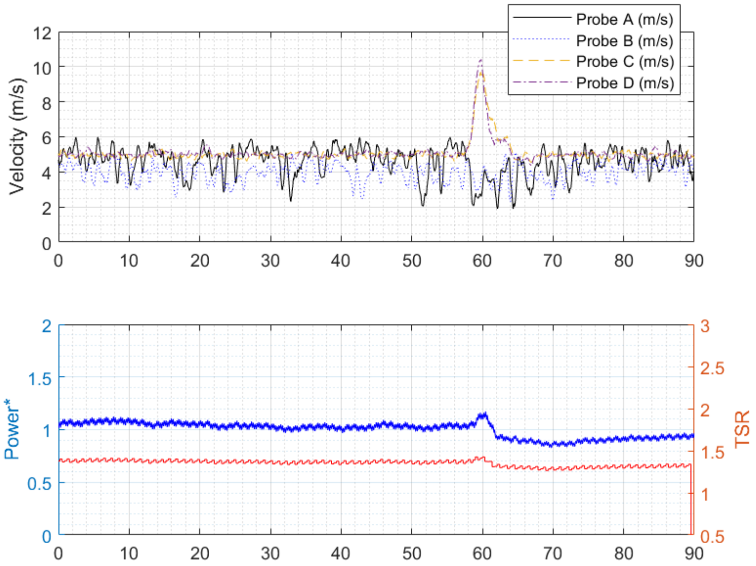
Probe A (m/s)
Probe B (m/s)
Probe C (m/s)
Probe D (m/s)
Velocity (m/s)
Power*
TSR

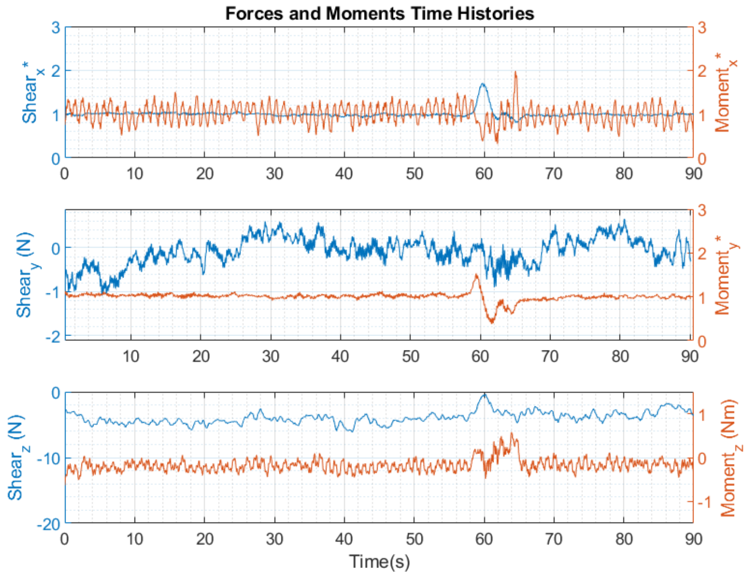

(b) negative EVS

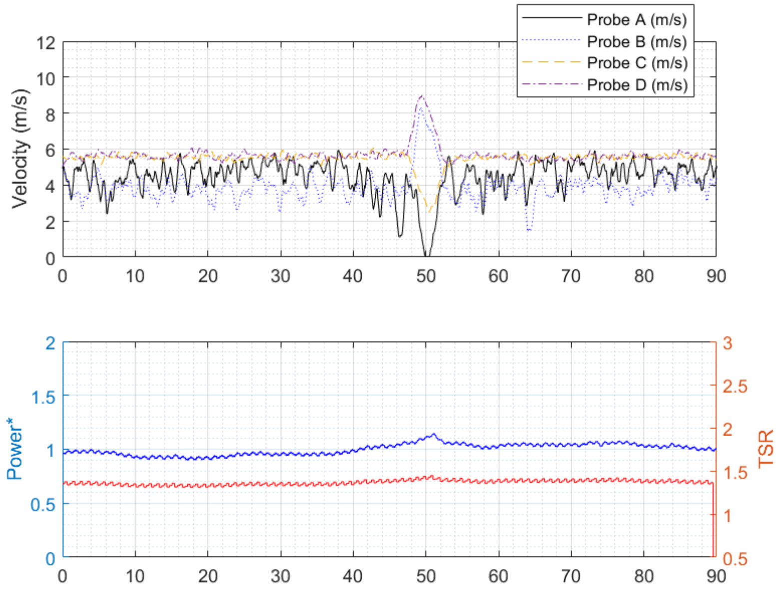

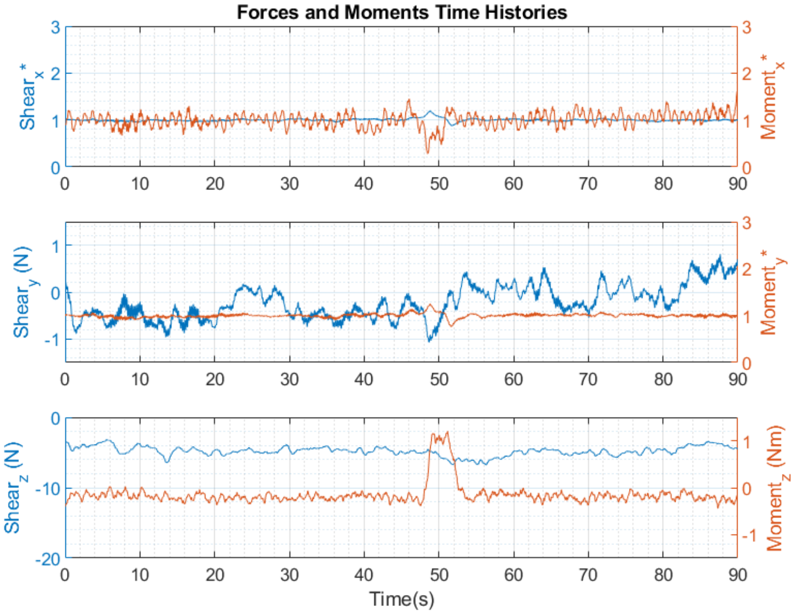

(c) EHS

Figure 3-6. The time history of the results from all the measuring instruments in (a) the EVS, (b) the negative EVS and (c) the EHS. The five sub-figures in order from top to bottom in each figure show the wind velocities from 4 cobra probes, the power performance of the turbine, the X, the Y and the Z forces and moments at the base of the tower. The stared axis indexes are normalized by their corresponding value from uniform case A

In the EHS case, the most important load component at the tower base can be the Z axis moment. The data shows this extreme condition induces a 1.2 Nm torsion on the structure; normalizing this value using equation 3-7 yields, 0.009414. For a full-scale wind turbine with 92 m diameter working in an average 10 m/s wind speed the induced yaw moment on the structure by an EHS event would be 351 kNm.

$$CM_z = \frac{M_z}{\frac{1}{2}\rho U^2 AD} \tag{3-7}$$

ρ is the density of the air, A is the swept area of the rotor and D is the diameter.

3.4.2 Unsteady EOG

The EOG was generated using IGVs. As the time histories of the measuring instruments suggest this uniform gust has the most noticeable effect on both power generation and loads. As the second window in Figure 3-7 shows, this event can dangerously increase the rotor rotational speed if no active or passive controlling systems are being used (the TSR is changing from $\sim 1\ to\ 1.33$). The electrical power generation might not be the proper quantity for comparison. The generator efficiency is highly dependent on the rotor speed. Therefore, as the rotor starts rotating faster and closer to nominal rotational speed of the generator, it becomes more efficient; here the electrical power increased 148% at the end of the gust event. The mechanical power should be a better quantity for comparison, which is highly dependent on the operational TSR. The rotor will generate different amount of torque in different TSRs. Therefore, a similar gust on a similar wind turbine can have different effects in different operating TSRs. The same applies for the loads.

The overall drag on the structure (X shear) and the main bending moment (Y moment) at the base, which is the main moment cause by the drag force, increased by 105% and 167 % respectively. Their difference depends on the hub height and the rotor diameter; in the current setup the average Y moment to the average X shear ratio is $\sim$1.55.

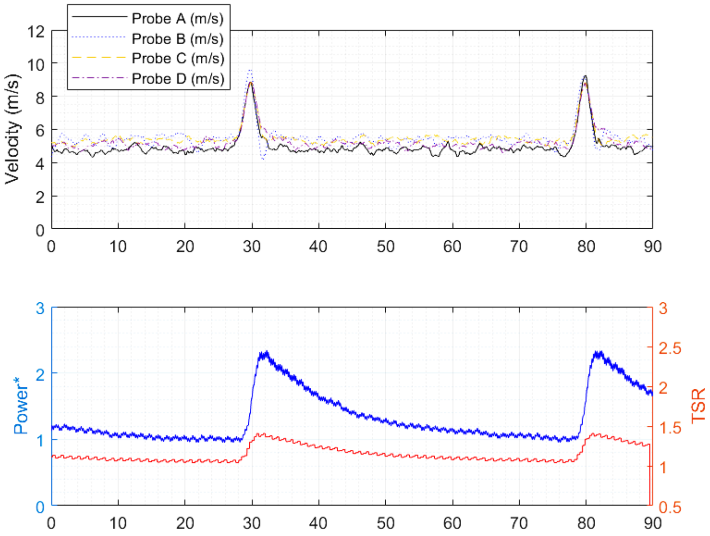

Figure 3-7. The time history of the results from all the probes in EOG using IGVs from top to bottom in order, the wind velocities from 4 cobra probes, power performance of the turbine, the forces and moments at the tower base, The stared axis indexes are normalized by their corresponding value from uniform case B

The loads usually have the same profile as the gust with the same order of rising and falling time. Although, the power generation peak happens at the end of the gust event and then slowly decays afterwards. From another point of view, the extractable energy in a gust with a specific amplitude and time duration partially accumulates in the rotor rotational momentum with the residue in form of higher instantaneous electrical power generation. After the gust event the stored momentum slowly decays by transforming into electrical power as it can be seen in the second window of the Figure 3-7.

The gust effects the X moment contributed by the rotor torque. Therefore, the sudden increase in the wind speed (gust) causes abrupt increase in the X moment which has approximately the same rising and falling time as the gust. the Y shear/ force again has no correlation with the gust. There is a slight correlation between Z force and the gust which results in a lift on the turbine (signal moves from negative values toward zero in the last sub-figure in Figure 3-7). Also, there is a rather large negative correlation between the Z moment and the gust that pushes and tilts the rotor up which induces a gyroscope moment

(~1.2 Nm) on the structure. Note that this effect highly depends on the structure of the wind turbine and might not happen in commercial HAWTs.

3.5 Conclusion

An experimental study has been carried out to investigate the effect of transient extreme operating conditions based on the IEC standard (specifically EWSs and EOG) tailored and scaled for a 2.2 HAWT at the WindEEE Dome at Western University. The main assumption used for the length and time scaling is that the duration of each extreme condition is equal to the propagation time of the four tip vortex loops in the wake. Other parameters were adjusted accordingly to accommodate for hardware limitations in generating the flow fields. Two uniform cases as the baselines for comparing the effect of different scenarios were carried also out.

The unsteady EVSs and EHS did not have any significant effect on the power performance and overall loading at the base of the turbine. Nevertheless, EHS induced a noticeable torsion on the structure.

The EOG affects the turbine significantly. Results showed that if no means of control for the rotor speed is considered the power generation and loadings can increase significantly with the highly dynamic behavior. Also, the reaction of the same wind turbine to the same EOG event can be different depending on the operational TSR. In the EOG event, the loading profiles are corelated with the shape of the gust event itself (the peak of the loads relatively are at the same point as the gust peak), but the power generation's peak happens at the end of the gust event.

Overall, this study presents an alternative experimental procedure for investigating the global loading and power generation of a scaled wind turbine under scaled deterministic transient wind conditions. The procedure has the potential to be improved and used for developing and testing new wind energy prototypes in transient conditions.

In future work, for the EVSs and EHS cases it is advisable to investigate the loads on the blades' roots and bearings as well as yaw bearing to implement a fatigue load analysis.

In the present study the TSR was determined from wake effect scaling and physical limits of the test apparatus, resulting in a TSR∼1.1. In future work, an attempt should be made to test the higher TSR through tests apparatus and controller modifications. Testing of the effect of different extreme events durations at different operating TSRs would help validate the suggested time scaling.

3.6 References

[1] McKinsey & Company, “Global Energy Perspective 2019 : Reference Case,” *Energy Insights,* no. January, p. 31, 2019.

[2] M. Anvari, G. Lohman, M. Wachter, P. Milan, E. Lorenz, D. Heinemann, M.R. Rahimi Tabar, J. Peinke, “Short term fluctuations of wind and solar power systems,” *New Journal of Physics*, vol. 18, no. 6, p. 063027, Jun. 2016, doi: 10.1088/1367-2630/18/6/063027. [3] P. Milan, M. Wächter, and J. Peinke, “Turbulent Character of Wind Energy,” *Physical Review Letters*, vol. 110, no. 13, p. 138701, Mar. 2013, doi: 10.1103/PhysRevLett.110.138701.

[4] T. Burton, N. Jenkins, D. Sharpe, and E. Bossanyi, *Wind Energy Handbook*, 2nd ed. Chichester, UK: John Wiley and Sons Ltd, 2011.

[5] A. Rezaeiha, R. Pereira, and M. Kotsonis, “Fluctuations of angle of attack and lift coefficient and the resultant fatigue loads for a large Horizontal Axis Wind turbine,” 2017, doi: 10.1016/j.renene.2017.07.101.

[6] Y. Feng, Y. Qiu, C. J. Crabtree, H. Long, and P. J. Tavner, “Monitoring wind turbine gearboxes,” *Wind Energy*, vol. 16, no. 5, pp. 728–740, Jul. 2013, doi: 10.1002/we.1521.

[7] E. A. Bossanyi, A. Kumar, and O. Hugues-Salas, “Wind turbine control applications of turbine-mounted LIDAR,” in *Journal of Physics: Conference Series*, 2014, vol. 555, no. 1, doi: 10.1088/1742-6596/555/1/012011.

[8] IEC, “(International Electrotechnical Commission) IEC 61400-1: Wind turbines - Part 1: Design requirements, 3rd ed.,” Geneva, Switzerland, 2005.

[9] IEC, “(International Electrotechnical Commission) IEC 61400-1: Wind energy generation systems - Part 1: Design requirements, 4th ed.,” Geneva, Switzerland, 2019.

[10] T. T. B. Wester, G. Kampers, G. Gulker, J. Peinke, U. Cordes, C. Tropea, M. Holling, “High speed PIV measurements of an adaptive camber airfoil under highly gusty inflow conditions,” in *Journal of Physics: Conference Series*, 2018, vol. 1037, no. 7, doi: 10.1088/1742-6596/1037/7/072007.

[11] V. Petrović, F. Berger, L. Neuhaus, M. Hölling, and M. Kühn, “Wind tunnel setup for experimental validation of wind turbine control concepts under tailor-made reproducible wind conditions,” in *Journal of Physics: Conference Series*, 2019, vol. 1222, no. 1, doi: 10.1088/1742-6596/1222/1/012013.

[12] L. Li, R. J. Hearst, M. A. Ferreira, and B. Ganapathisubramani, “The near-field of a lab-scale wind turbine in tailored turbulent shear flows,” *Renewable Energy*, vol. 149, pp. 735–748, 2020, doi: https://doi.org/10.1016/j.renene.2019.12.049.

[13] N. Sezer-Uzol and O. Uzol, “Effect of steady and transient wind shear on the wake structure and performance of a horizontal axis wind turbine rotor,” *Wind Energy*, vol. 16, no. 1, pp. 1–17, Jan. 2013, doi: 10.1002/we.514.

[14] A. Albers, T. Jakobi, R. Rohden, and J. Stoltenjohannes, “Influence of meteorological variables on measured wind turbine power curves,” in *European Wind Energy Conference and Exhibition 2007, EWEC 2007*, 2007, vol. 3.

[15] M. Wächter, H. Heibelmann, M. Holling, A. Morales, P. Milan, T. Mucke, J. Peinke, N. Reinke, P. Rinn,“The turbulent nature of the atmospheric boundary layer and its impact on the wind energy conversion process,” *Journal of Turbulence*, vol. 13, pp. 1–21, 2012, doi: 10.1080/14685248.2012.696118.

[16] J. Schottler, N. Reinke, A. Hölling, J. Whale, J. Peinke, and M. Hölling, “On the impact of non-Gaussian wind statistics on wind turbines – an experimental approach,” *Wind Energy Science*, vol. 2, no. 1, 2017, doi: 10.5194/wes-2-1-2017.

[17] H. Hangan, M. Refan, C. Jubayer, D. Romanic, D. Parvu, J. LoTufo, and A. Costache, “Novel techniques in wind engineering,” *Journal of Wind Engineering and Industrial Aerodynamics*, vol. 171, pp. 12–33, Dec. 2017, doi: 10.1016/j.jweia.2017.09.010.

[18] TFI Ltd., “Cobra Probe,” *Turbulent Flow Instrumentation Pty Ltd*, 2011. https://www.turbulentflow.com.au/Products/CobraProbe/CobraProbe.php (accessed Jun. 12, 2020).

[19] S. B. Pope, *Turbulent scalar mixing processes*, vol. 21, no. 1. Cambridge University Press, 2000.

Chapter 4

4 Concluding Remarks and Future Work

Wind energy is one of the primary solutions to transition to a GHG free electricity generation with high potential around the world and especially in Canada. While this transition is mainly driven by societal and climate change impacts, the main key for this market to grow more in the future is further lowering LCOE. This is further dependent on having more reliable wind energy systems that can withstand extreme wind conditions throughout their lifetime.

This research aimed to physically simulate these types of conditions as specified in the IEC 61400-1 standard. Experimental simulation of these transient events generates reliable data for scholars in the wind energy to assess various design concepts in terms of both performance and reliability. The research was performed in two parts: (I) Generic transient extreme wind inflow conditions were reproduced in the WindEEE Dome. The setups for the 60 fans in the WindEEE Dome were derived based on a set of preliminary CFD simulations. Based on these simulations generic representations of the various IEC standard extreme wind conditions were physically generated, and for the first time scaled to be representative for a model HAWT (Chapter 2). (II) These extreme events were applied on the model HAWT to investigate their effects in terms of the power and load performance of the turbine (Chapter 3). The performance of the model HAWT under extreme conditions were compared with its performance under uniform inflows.

The original outputs of the research are: (I) The physically simulation of IEC extreme wind conditions by controlling a matrix of fans. (II) The definition of a new scaling method for wind tunnel testing of HAWT models. (III) The comparison of performance and dynamic loading of HAWT under extreme gust conditions and uniform inflows. (IV) Developing a time efficient numerical model of the WindEEE test chamber in straight flow mode using the 60 fans wall. The combination between CFD preliminary setup simulations and the physical inflow simulations was deemed to be important given the non-linearities in the multiple-fan flow field. This hybrid numerical/ experimental approach in creating gusts, saved a significant amount of time in the trial and error process of the flow modulation.

Future work recommendations: (I) Further unsteady CFD simulations can be perform that includes the recirculation pass in the outer shell. This would give more insight about flow recirculation in WindEEE dome in the straight 2D flow mode. Especially, when applying uneven dynamic changes in the fan powers. (II) When generating EVS and EHS, for the fan controls a time lag should be taken into account due to differences in velocities at upper and lower peak. This can be eliminated by considering the 12.5m distance from the fans to the test point and the magnitude of the peak velocities in the desired EWS. (III) The EVS, EHS and EOG events super imposed on ABL flows can be generated; in this study the background flows were uniform. (IV) The exploration of other loads under EWSs and EOG conditions such as fatigue loads on individual blade roots, bearings and nacelle. This can generate a validation data base for structure analysis and help developing more precise design load case under these conditions.

Curriculum Vitae

Name:	Kamran Shirzadeh Ajirlo
Post-secondary Education and Degrees:	Shahid Beheshti University (SBU) Tehran, Iran Bachelor of Science in Fluid Mechanics, 2012 – 2016 Western University, London, Ontario, Canada MSc in Mechanical Eng., 2018-2020
Honours and Awards:	Accepted as a competence Student for Master Program without entrance exam. Shahid Beheshti University 2016 Western Graduate Research Scholarship, 2018-2020
Related Work Experience:	University of Western Ontario (UWO) Teaching Assistant, 2018-2020